

Bayesian Clustering via Fusing of Localized Densities

Alexander Dombowsky¹ and David B. Dunson^{1,2}

¹Department of Statistical Science, Duke University, Durham, NC, USA

²Department of Mathematics, Duke University, Durham, NC, USA

Abstract

Bayesian clustering typically relies on mixture models, with each component interpreted as a different cluster. After defining a prior for the component parameters and weights, Markov chain Monte Carlo (MCMC) algorithms are commonly used to produce samples from the posterior distribution of the component labels. The data are then clustered by minimizing the expectation of a clustering loss function that favours similarity to the component labels. Unfortunately, although these approaches are routinely implemented, clustering results are highly sensitive to kernel misspecification. For example, if Gaussian kernels are used but the true density of data within a cluster is even slightly non-Gaussian, then clusters will be broken into multiple Gaussian components. To address this problem, we develop Fusing of Localized Densities (FOLD), a novel clustering method that melds components together using the posterior of the kernels. FOLD has a fully Bayesian decision theoretic justification, naturally leads to uncertainty quantification, can be easily implemented as an add-on to MCMC algorithms for mixtures, and favours a small number of distinct clusters. We provide theoretical support for FOLD including clustering optimality under kernel misspecification. In simulated experiments and real data, FOLD outperforms competitors by minimizing the number of clusters while inferring meaningful group structure.

Keywords— Bayes; Clustering; Decision theory; Kernel misspecification; Mixture models; Statistical distances

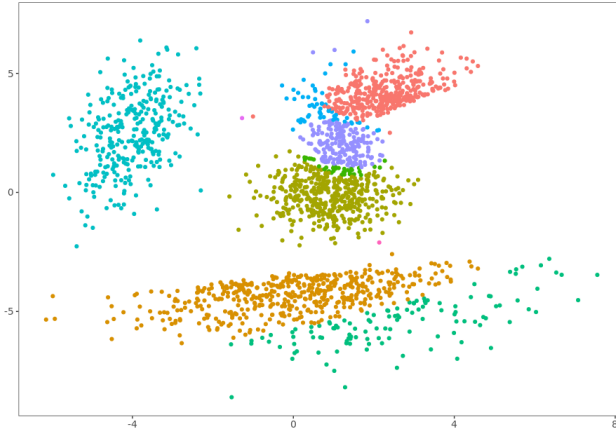


Figure 1: An example of over-clustering. A Bayesian Gaussian mixture model with 10 components and Dirichlet prior concentration parameter equal to $1/10$ is fit to data generated from a mixture of skew Gaussian distributions with overlapping densities.

1 Introduction

Clustering data into groups of relatively similar observations is a canonical task in exploratory data analysis. Algorithmic clustering methods, such as k-means, k-medoids, and hierarchical clustering, rely on dissimilarity metrics, an approach which is often heuristic but may perform well in practice; see [Hastie et al. \(2009\)](#), [Jain \(2010\)](#), and [Kiselev et al. \(2019\)](#) for an overview. In comparison, model-based clustering methods utilize mixtures of probability kernels to cluster data, ordinarily by inferring the component labels ([Fraley and Raftery, 2002](#)). Choices of kernel depend on the type of data being considered, with the Gaussian mixture model (GMM) particularly popular for continuous data. A conceptual advantage of model-based methods is the ability to express uncertainty in clustering. For example, the expectation-maximization (EM) algorithm uses maximum likelihood estimates of the component-specific parameters and weights to calculate each observations' posterior component allocation probabilities, which are interpreted as a measure of clustering uncertainty ([Bensmail et al., 1997](#)). As estimation of the weights and component-specific parameters is crucial for model-based clustering, there is a wide literature on quantifying rates of convergence for various mixture models, which is usually expressed in terms of the mixing measure (see [Guha et al., 2021](#) and references therein).

Bayesian mixture models have received increased attention as a clustering method in recent years. The Bayesian framework can account for uncertainty in the number of components and incorporate prior information on the component-specific parameters, with Markov chain Monte Carlo (MCMC) algorithms employed to generate posterior samples for the mixture weights, kernel parameters, and component labels for each data point. Based on posterior samples of the component labels, one can obtain Monte Carlo approximations to Bayes clustering estimators. For d -dimensional data $\mathbf{X} = (X_1, \dots, X_n)$, the Bayes estimator \mathbf{c}^* is the minimizer of an expected loss function conditional on \mathbf{X} over all possible clusterings $\mathbf{c} = (c_1, \dots, c_n)$. There are several popular choices of loss, including Binder's ([Binder, 1978](#)) and Variation of Information (VI) ([Meilă, 2007](#)), which are distance metrics over the space of

partitions and favour clusterings that are similar to the component labels. Further details on set partitions and their role in Bayesian clustering can be found in [Meilă \(2007\)](#), [Wade and Ghahramani \(2018\)](#), and [Paganin et al. \(2021\)](#). Several measures of uncertainty in clustering with Bayesian mixtures exist, including the posterior similarity matrix and credible balls of partitions ([Wade and Ghahramani, 2018](#)).

However, model-based clustering approaches, including Bayesian implementations, can be brittle in applications due to unavoidable impacts of kernel misspecification. Mixtures will often induce over-clustering in this setting by dividing dense groups of observations whose empirical density cannot be approximated by members of the assumed kernel family. An example of this phenomena is shown in [Figure 1](#), where a 10 component Bayesian GMM is fit to data generated from a mixture of bivariate skew Gaussian distributions. Despite using a concentration parameter of 1/10 in the symmetric Dirichlet prior to induce a small number of clusters ([Rousseau and Mengersen, 2011](#)), the GMM allocates the data into 10 poorly defined groups. A group of observations in the bottom third of the sample space is split into two, while several observations are placed into their own groups despite being near dense collections of data.

Several approaches have been proposed to address the issue of over-clustering due to kernel misspecification. A natural solution is to define a flexible class of kernels, exemplified by the mixtures in [Karlis and Santourian \(2009\)](#), [Juárez and Steel \(2010\)](#), [O’Hagan et al. \(2016\)](#), [Tortora et al. \(2019\)](#), and [Dang et al. \(2023\)](#). To increase flexibility further, [Rodríguez and Walker \(2014\)](#) propose a mixture of nonparametric unimodal kernels. Similarly, [Bartolucci \(2005\)](#), [Li \(2005\)](#), [Di Zio et al. \(2007\)](#), and [Malsiner-Walli et al. \(2017\)](#) use carefully chosen mixtures of Gaussians to characterize the data within each cluster. However, there is an unfortunate pitfall with the general strategy of using flexible families of kernels. In particular, as the flexibility of the kernel increases, identifiability and optimal estimation rates for inferring the mixing measure tend to weaken, especially when the true number of mixture components is unknown ([Nguyen, 2013](#); [Ho and Nguyen, 2016a](#); [Heinrich and Kahn, 2018](#)). Even the transition from location Gaussian kernels with known covariance to location-scale Gaussian kernels can have substantial consequences on the convergence rate of the component means ([Manole and Ho, 2022](#)). Such problems motivated [Ho et al. \(2020\)](#) to propose an alternative estimator of the mixing measure that is more robust than maximum likelihood and Bayesian approaches and can achieve optimal convergence rates.

Alternatively, one can develop generalized Bayesian methods of clustering that avoid defining a fully generative probabilistic model for the data. For example, [Duan and Dunson \(2021\)](#) propose to conduct model-based clustering based on a pairwise distance matrix instead of the data directly to reduce sensitivity to kernel misspecification. [Rigon et al. \(2023\)](#) instead define a Gibbs posterior for clustering incorporating a clustering loss function in place of a likelihood function, completely bypassing modeling of the data. An alternative that maintains a fully generative model while robustifying inferences to misspecification is to use a coarsened posterior ([Miller and Dunson, 2019](#); [Gorsky et al., 2023](#)). This coarsening approach often has good practical performance in reducing over-clustering due to kernel misspecification.

Unfortunately, these approaches for accommodating kernel misspecification have various drawbacks. Along with slower convergence rates, flexible kernels typically require a large number of parameters, worsening the already burdensome computational cost of Bayesian

clustering. The generalized Bayes approaches can perform well in certain settings. However, both Gibbs posteriors and coarsened posteriors are highly sensitive to key tuning parameters, which can be difficult to choose objectively in practice.

A key advance is given in [Aragam et al. \(2020\)](#), which attempts to solve the problem of clustering based on a mixture model by merging components in a Gaussian mixture. They rely on a two-stage procedure that lacks uncertainty quantification and assumes that the true number of kernels is known. However, the approach of viewing clusters as arising from merging closely overlapping kernels is promising. Related merging ideas have been implemented in both frequentist and Bayesian approaches in a variety of settings, and several algorithms exist for deciding how and when to combine components together ([Chan et al., 2008](#); [Baudry et al., 2010](#); [Hennig, 2010](#); [Melnykov, 2016](#); [Guha et al., 2021](#); [Manole and Khalili, 2021](#)).

In this paper, we propose a novel decision theoretic method for Bayesian clustering that mitigates the effects of model misspecification. Let $X_1, \dots, X_n \sim f_0$, where f_0 is an unknown true probability density. Suppose we model the data with a Bayesian mixture model, with L components, component labels $\mathbf{s} = (s_1, \dots, s_n)$, component-specific atoms $\theta_1, \dots, \theta_L$, and kernels $g(\theta_1), \dots, g(\theta_L)$. Rather than focusing on \mathbf{s} , we compute clusters with the localized densities $\{g(\theta_{s_i})\}_{i=1}^n$. We define a loss function for any clustering $\hat{\mathbf{c}}$ that favours allocating i and j to the same cluster when the Hellinger distance between the densities $g(\theta_{s_i})$ and $g(\theta_{s_j})$ is small, encouraging grouping observations with overlapping component kernels. We cluster X_1, \dots, X_n with a Bayes estimator, interpreted as a Fusing of Localized Densities (FOLD). Our method has a fully decision theoretic justification, leads to interpretable uncertainty quantification, and can be readily implemented using the output of existing MCMC algorithms for mixtures.

Though previous methods have utilized merging kernels to account for kernel misspecification, to our knowledge none have a formal Bayesian decision theoretic justification. Although FOLD requires combinatorial optimization, we employ a method for speeding up computation based on hierarchical clustering of the Hellinger distances between the localized densities. We show concentration of the joint posterior for the weights and atoms as a byproduct of contraction of the mixing measure ([Nguyen, 2013](#); [Ho and Nguyen, 2016b](#); [Guha et al., 2021](#)). This allows us to show clustering optimality of FOLD in misspecified and well-specified kernel regimes.

In [Section 2](#), we explain our clustering method from a Bayesian decision theoretic perspective, provide a framework for uncertainty quantification, and demonstrate how to implement FOLD in practice. In [Section 3](#), we show asymptotic concentration of FOLD for misspecified kernel regimes. We evaluate FOLD against other model-based clustering methods on simulated examples in [Section 4](#), and consider an application to a cell line data set in [Section 5](#). Finally, we provide concluding remarks and some extensions in [Section 6](#).

2 Clustering with Localized Densities

2.1 Notation and Setup

Let $X_i = (X_{i1}, \dots, X_{id}) \in \mathbb{R}^d$ be multivariate observations, collected into $\mathbf{X} = (X_1, \dots, X_n)$. Assume that X_1, \dots, X_n are generated from an unknown mixture model: $X_i \sim f_0$, where $f_0 = \sum_{k=1}^{K_0} \pi_{0k} \tau_{0k}$, $\pi_{0k} > 0$ for $k = 1, \dots, K_0$, $\sum_{k=1}^{K_0} \pi_{0k} = 1$, and $K_0 < \infty$. Since f_0 is a mixture, the data generating process can be equivalently stated with the addition of latent variables $s_{0i} \in \{1, \dots, K_0\}$, so that $(X_i | s_{0i}) \sim \tau_{0s_{0i}}$ for all $i = 1, \dots, n$. \mathbb{P}_0 refers to probability and convergence statements with respect to the true data generating process, with $\mathbb{P}_0(A) = \int_A f_0(x) dx$ for any set A and $\mathbb{E}_0 \{\phi(X)\} = \int_{\mathbb{R}^d} \phi(x) f_0(x) dx$ for any function ϕ .

Let Θ denote a parameter space and $\mathcal{G} = \{g(\theta) : \theta \in \Theta\}$ be a family of continuous parametric probability distributions with supports on \mathbb{R}^d . Suppose a Bayesian mixture model over \mathcal{G} is fit to \mathbf{X} : $X_i \sim f$, where $f = \sum_{l=1}^L a_l g(\theta_l)$ and $\boldsymbol{\theta} = (\theta_1, \dots, \theta_L)$. We set $\lambda = \sum_{l=1}^L a_l \delta_{\theta_l}$ as the mixing measure associated with f , with δ_{θ} a degenerate measure concentrated at the atom θ , and will occasionally use the notation $f^{(\lambda)}$ instead of f to reflect this dependence. For all parameters, $\Pi(\cdot)$ is the prior distribution and $\Pi(\cdot | \mathbf{X})$ is the posterior distribution. We are primarily motivated to address the misspecified kernel case, in which $\tau_{0k} \neq g(\theta_l)$ for any choice of θ_l . However, our method can be applied to the well-specified case as well.

Let $\mathbf{s} = (s_1, \dots, s_n)$, $s_i \in \{1, \dots, L\}$, be component labels, inducing the partition $S = \{S_1, \dots, S_L\}$ of $\{1, \dots, n\}$. Exchangeable priors on partitions are referred to as Exchangeable Partition Probability Functions (EPPFs) (Pitman, 1995). If $\Pi(\mathbf{s})$ is an EPPF then only the sizes $|S_1|, \dots, |S_L|$ and number of non-empty partition sets impact the prior probability $\Pi(\mathbf{s})$. Assuming the prior for the atoms is independent of the labels, we obtain the joint posterior,

$$\Pi(\mathbf{s}, \boldsymbol{\theta} | \mathbf{X}) \propto \Pi(\mathbf{s}) \Pi(\boldsymbol{\theta}) \prod_{i=1}^n g(X_i; \theta_{s_i}). \quad (1)$$

There is a rich literature on MCMC algorithms for sampling from (1). There are many choices of $\Pi(\mathbf{s})$ that can be used in practice, ranging from the EPPF corresponding to a finite symmetric Dirichlet prior to more elaborate choices such as the Pitman-Yor. Regardless of the choice of $\Pi(\mathbf{s})$, when the prior distribution on the atoms is conjugate to \mathcal{G} , Gibbs sampling tends to be the most popular choice for posterior sampling.

To cluster \mathbf{X} , we typically calculate the Bayes estimator with respect to a clustering loss function that favours similarity to \mathbf{s} . A decision theoretic approach to Bayesian clustering was proposed in Binder (1978), which introduced Binder’s loss function. This loss penalizes allocating two observations to the same cluster when they are generated from different mixture components (and vice versa), and is thoroughly examined in Lau and Green (2007). Wade and Ghahramani (2018) advocates for the Variation of Information (VI) loss (Meilá, 2007), which is motivated by information theory and often produces a smaller number of clusters than Binder’s loss. Generalized versions of Binder’s and VI loss are proposed in Dahl et al. (2022), and tend to improve performance. Various statistical software packages exist to obtain Bayesian clustering estimators under these losses using samples from $\Pi(\mathbf{s} | \mathbf{X})$ as input, including `mcclust` (Fritsch, 2022), `mcclust.ext` (Wade, 2015), and `salso` (Dahl et al., 2020).

2.2 Decision Theory Formulation

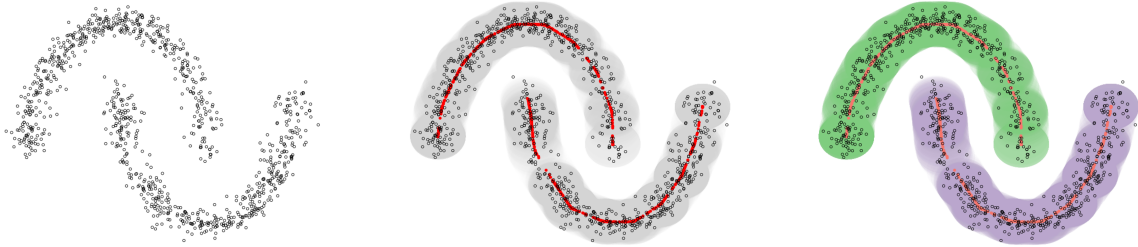


Figure 2: A Bayesian location Gaussian mixture is fit to a version of the `moons` data set from the `RSSL` package (Krijthe and Loog, 2015; Krijthe, 2016). The localized densities are inferred using an MCMC algorithm, then melded together into clusters based on their pairwise Hellinger distance.

We aim to estimate a clustering $\hat{\mathbf{c}} = (\hat{c}_1, \dots, \hat{c}_n)$ of \mathbf{X} and partition $\hat{\mathbf{C}} = \{\hat{C}_1, \dots, \hat{C}_{\hat{K}_n}\}$ based on merging components from the posterior (1) that have similar kernels $g(\theta_l)$. The motivation here is to remedy the cluster splitting that occurs in using multiple parametric kernels $g(\theta_l)$ to represent each ‘true’ kernel τ_{0k} . We refer to $\{g(\theta_{s_i})\}_{i=1}^n$ as *localized densities*, corresponding to the density of each data point, $(X_i | s_i, \boldsymbol{\theta}) \sim g(\theta_{s_i})$, under the assumed mixture model being fit to the data.

To counteract cluster splitting, we will define the loss of assigning two observations into the same or different group as a function of the statistical distance between their localized densities. This loss is motivated by the notion that data generated from the same τ_{0k} will tend to be assigned overlapping kernels under the misspecified mixture. Figure 2 shows the behaviour of the posterior distributions of the localized densities when the model $f = \sum_{l=1}^{30} a_l \mathcal{N}_2(\theta_l, 0.02\mathbf{I}_2)$ is fit to a version of the `moons` data. The red points plot $\mathbb{E}_{\Pi}(\theta_{s_i} | \mathbf{X})$ for each $i = 1, \dots, n$, with gray circles representing the 95% high density regions of a $\mathcal{N}_2(\mathbb{E}_{\Pi}(\theta_{s_i} | \mathbf{X}), 0.02\mathbf{I}_2)$ distribution. The crescent clusters are split into multiple overlapping Gaussian kernels, but are recovered by fusing these kernels together.

We define the loss of any clustering $\hat{\mathbf{c}}$ resulting from the component labels \mathbf{s} of a mixture over \mathcal{G} to be

$$\mathcal{L}_{\mathcal{G}}(\hat{\mathbf{c}}, \mathbf{s}) = \sum_{i < j} \{ \mathbf{1}_{\hat{c}_i = \hat{c}_j} \mathcal{H}_{ij} + \omega \mathbf{1}_{\hat{c}_i \neq \hat{c}_j} (1 - \mathcal{H}_{ij}) \}, \quad (2)$$

where $\omega > 0$ and $\mathcal{H}_{ij} = h \{g(\theta_{s_i}), g(\theta_{s_j})\}$ is the Hellinger distance (Hellinger, 1909) between $g(\theta_{s_i})$ and $g(\theta_{s_j})$. Observe that $\mathcal{L}_{\mathcal{G}}(\hat{\mathbf{c}}, \mathbf{s}; \boldsymbol{\theta})$ is non-negative for any $\hat{\mathbf{c}}$ since $\mathcal{H}_{ij} \in [0, 1]$. The loss of assigning $\hat{c}_i = \hat{c}_j$ is \mathcal{H}_{ij} . If $s_i = s_j$, then there is no loss incurred. When $s_i \neq s_j$, the loss will remain small when the kernels $g(\theta_{s_i}), g(\theta_{s_j})$ are similar under the Hellinger distance. Conversely, allocating i and j to different clusters results in a loss of $\omega(1 - \mathcal{H}_{ij})$. If $\mathcal{H}_{ij} = 1$, which occurs when the supports of $g(\theta_{s_i})$ and $g(\theta_{s_j})$ are disjoint, then setting $\hat{c}_i \neq \hat{c}_j$ accumulates zero loss. Otherwise, the loss depends on the Hellinger separation between the localized densities and the loss parameter ω .

Our loss $\mathcal{L}_g(\widehat{\mathbf{c}}, \mathbf{s}; \boldsymbol{\theta})$ is invariant to permutations of the data indices and of the labels in either $\widehat{\mathbf{c}}$ or \mathbf{s} , which is desirable for clustering losses (Binder, 1978). In addition, $\mathcal{L}_g(\widehat{\mathbf{c}}, \mathbf{s}; \boldsymbol{\theta})$ is a continuous relaxation of Binder’s loss,

$$\mathcal{L}_B(\widehat{\mathbf{c}}, \mathbf{s}) = \sum_{i < j} \{ \mathbf{1}_{\hat{c}_i = \hat{c}_j} \mathbf{1}_{s_i \neq s_j} + \omega \mathbf{1}_{\hat{c}_i \neq \hat{c}_j} \mathbf{1}_{s_i = s_j} \}. \quad (3)$$

A key property of Binder’s loss is that it is a quasimetric over the space of partitions (Wade and Ghahramani, 2018; Dahl et al., 2022). $\mathcal{L}_g(\widehat{\mathbf{c}}, \mathbf{s}; \boldsymbol{\theta})$ is not a quasimetric in general, but instead aims to mitigate the problem of cluster splitting arising under kernel misspecification. One can show that $\mathcal{L}_g(\widehat{\mathbf{c}}, \mathbf{s}; \boldsymbol{\theta})$ can be rewritten as the sum of $\mathcal{L}_B(\widehat{\mathbf{c}}, \mathbf{s})$ and a remainder term $\mathcal{B}_G(\widehat{\mathbf{c}}, \mathbf{s})$, and that $\mathcal{L}_G(\mathbf{s}, \mathbf{s}) = 0$ only when the components of f are completely separated. The closed form of the remainder $\mathcal{B}_G(\widehat{\mathbf{c}}, \mathbf{s})$ is given in Appendix A.1, and is interpreted as an added cost to Binder’s loss that encourages merging components.

Proposition 1. Let $\mathcal{L}_g(\widehat{\mathbf{c}}, \mathbf{s}; \boldsymbol{\theta})$ be the loss function defined in (2) and $\mathcal{L}_B(\widehat{\mathbf{c}}, \mathbf{s})$ be the form of Binder’s loss in (3). Then,

$$\mathcal{L}_g(\widehat{\mathbf{c}}, \mathbf{s}; \boldsymbol{\theta}) = \mathcal{L}_B(\widehat{\mathbf{c}}, \mathbf{s}) + \mathcal{B}_G(\widehat{\mathbf{c}}, \mathbf{s}), \quad (4)$$

where $\mathcal{B}_G(\mathbf{s}, \mathbf{s}) = 0$ if and only if $h(g(\theta_m), g(\theta_l)) = 1$ for all component pairs $m, l = 1, \dots, L$.

The parameter ω on the second term in our loss calibrates separation of the clusters. For example, suppose we compare the clustering $\widehat{\mathbf{c}}_1$, which includes clusters \hat{C}_h and \hat{C}_k , with the clustering $\widehat{\mathbf{c}}_2$, which is equivalent to $\widehat{\mathbf{c}}_1$ but now contains the merged cluster $\hat{C}_h \cup \hat{C}_k$. The difference in their losses is

$$\mathcal{L}_G(\widehat{\mathbf{c}}_1, \mathbf{s}) - \mathcal{L}_G(\widehat{\mathbf{c}}_2, \mathbf{s}) = \omega \sum_{i \in \hat{C}_h, j \in \hat{C}_k} (1 - \mathcal{H}_{ij}) - \sum_{i \in \hat{C}_h, j \in \hat{C}_k} \mathcal{H}_{ij}.$$

The loss of $\widehat{\mathbf{c}}_2$ is less than that of $\widehat{\mathbf{c}}_1$ when

$$\frac{1}{|\hat{C}_h| |\hat{C}_k|} \sum_{i \in \hat{C}_h, j \in \hat{C}_k} \mathcal{H}_{ij} < \gamma := \frac{\omega}{1 + \omega}. \quad (5)$$

This implies that large values of ω promote fusing clusters, while smaller values lead to more clusters having less between-cluster heterogeneity. When $\widehat{\mathbf{c}}_1 = \mathbf{s}$, it is clear that a smaller loss can be attained by merging components with average pairwise Hellinger distance less than γ . Trivial clusterings are favoured when ω is taken to its lower and upper limits, similar to both Binder’s loss and the VI loss (Wade and Ghahramani, 2018; Dahl et al., 2022). As $\omega \rightarrow 0$, our loss is minimized in placing each observation in its own cluster, while, as $\omega \rightarrow \infty$, all observations are placed in a single cluster.

The risk of any clustering $\widehat{\mathbf{c}}$ is the posterior expectation of its loss, which integrates over the uncertainty in the labels and atoms after observing the data;

$$\begin{aligned} \mathcal{R}_G(\widehat{\mathbf{c}} \mid \mathbf{X}) &= \mathbb{E}_\Pi \{ \mathcal{L}_g(\widehat{\mathbf{c}}, \mathbf{s}; \boldsymbol{\theta}) \mid \mathbf{X} \} \\ &= \sum_{i < j} \{ \mathbf{1}_{\hat{c}_i = \hat{c}_j} \Delta_{ij} + \omega \mathbf{1}_{\hat{c}_i \neq \hat{c}_j} (1 - \Delta_{ij}) \}, \end{aligned} \quad (6)$$

where $\Delta_{ij} = \mathbb{E}_{\Pi}(\mathcal{H}_{ij} \mid \mathbf{X})$ is the expected Hellinger distance between the localized densities $g(\theta_{s_i})$ and $g(\theta_{s_j})$ for observations i and j , respectively. The point estimator of the clustering of \mathbf{X} is given by the Bayes estimator, denoted \mathbf{c}_{FOLD} , which is the minimizer of (6) over the space of all possible cluster allocations of $\{1, \dots, n\}$,

$$\mathbf{c}_{\text{FOLD}} = \underset{\hat{\mathbf{c}}}{\operatorname{argmin}} \mathcal{R}_{\mathcal{G}}(\hat{\mathbf{c}} \mid \mathbf{X}). \quad (7)$$

The expected Hellinger distance terms in the risk (6) have several appealing properties that distinguish FOLD from quasimetric loss approaches. We collect these terms into a matrix and show that they exhibit bounded and metric properties in the following proposition.

Proposition 2. Let $\Delta = (\Delta_{ij})_{i,j}$, where $\Delta_{ij} = \mathbb{E}_{\Pi}(\mathcal{H}_{ij} \mid \mathbf{X})$. Then Δ satisfies the following with \mathbb{P}_0 -probability equal to 1 for all $i, j, h = 1, \dots, n$:

1. $0 \leq \Delta_{ij} \leq 1$.
2. $\Delta_{ii} = 0$, $\Delta_{ji} = \Delta_{ij}$, and $\Delta_{ih} \leq \Delta_{ij} + \Delta_{jh}$.
3. $\Delta_{ij} \leq \Pi(s_i \neq s_j \mid \mathbf{X})$.

The boundedness and symmetry of the Hellinger distance are preserved after taking the posterior expectation, implying that $\mathcal{R}_{\mathcal{G}}(\hat{\mathbf{c}} \mid \mathbf{X})$ is non-negative for any clustering and that the sum in (6) may be taken over the indices $i < j$. We can also deduce from these properties that FOLD will induce coarser clusterings than Binder’s loss. Similar to (5), one can show that Binder’s loss prefers assigning i and j to the same cluster when $\Pi(s_i \neq s_j \mid \mathbf{X}) < \gamma$. If $\Delta_{ij} < \gamma < \Pi(s_i \neq s_j \mid \mathbf{X})$, FOLD will disagree with usual Bayesian model-based clustering under Binder’s loss, with FOLD preferring to merge i and j into the same cluster.

2.3 Uncertainty Quantification

In the previous section, we discussed obtaining an estimated clustering \mathbf{c}_{FOLD} by minimizing the expectation of $\mathcal{L}_{\mathcal{G}}(\hat{\mathbf{c}}, \mathbf{s}; \boldsymbol{\theta})$ over $\Pi(\mathbf{s}, \boldsymbol{\theta} \mid \mathbf{X})$, and contrasted our approach with the clusterings given by Binder’s and the VI loss. Under these latter loss functions, one implicitly assumes that the best clustering of the data is given by the component labels \mathbf{s} . Hence, the value of a Bayes estimator \mathbf{c}^* corresponding to these losses can be interpreted as capturing some notion of centrality for the posterior $\Pi(\mathbf{s} \mid \mathbf{X})$, akin to minimizing the squared error loss when estimating a real-valued parameter. In applications of Bayesian clustering to real data, we often find that there is substantial uncertainty in the component labels a posteriori. To avoid overstating the significance of \mathbf{c}^* , it is thus important to express this uncertainty in a clear and interpretable manner.

A standard choice of uncertainty quantification is the posterior similarity matrix (PSM) $P = \{\Pi(s_i = s_j \mid \mathbf{X})\}_{i,j}$, with entries ordered by the labels in \mathbf{c}^* and visualized as a heatmap. The PSM measures the posterior probability of two observations being allocated to the same mixture component. When ordered by \mathbf{c}^* , this gives an idea of the uncertainty of clustering assignment within and between clusters. However, P can under-represent uncertainty in \mathbf{c}^* (Wade and Ghahramani, 2018) and differs from typical notions of uncertainty quantification in Bayesian inference, such as credible intervals for real-valued parameters. One can also

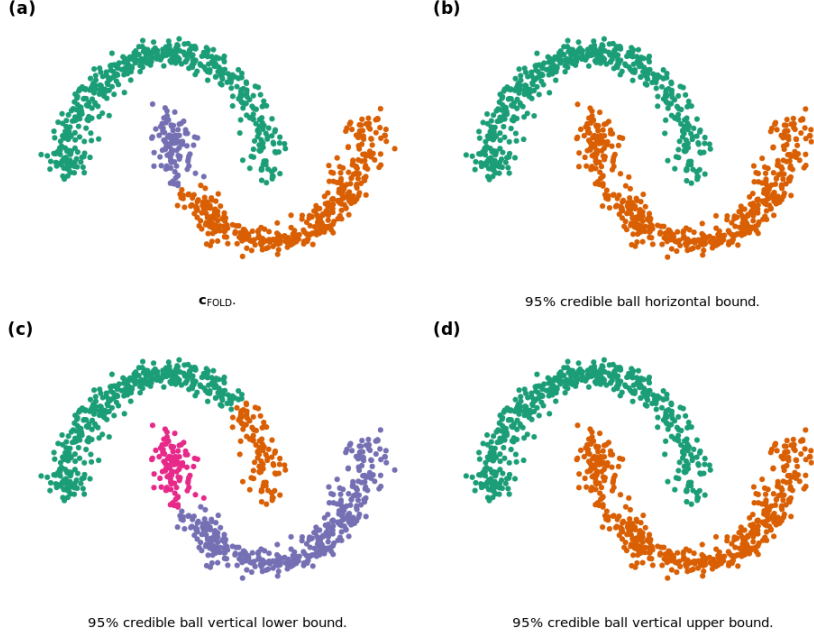


Figure 3: A clustering \mathbf{c}_{FOLD} of the moons data, with $\omega = 118.2$, is shown in (a). (b)-(d) display the horizontal, vertical lower, and vertical upper bounds of the 95% credible ball, with $D(\cdot, \cdot)$ as the VI loss.

quantify uncertainty with a set of high probability groupings that are close to \mathbf{c}^* under a partition distance $D(\cdot, \cdot)$. This notion is formalized by creating a 95% credible ball around \mathbf{c}^* , defined by the smallest radius $\epsilon \geq 0$ with $\Pi\{D(\mathbf{c}^*, \mathbf{s}) \leq \epsilon \mid \mathbf{X}\} \geq 0.95$ (Wade and Ghahramani, 2018). Since \mathbf{c}^* roughly corresponds to the centre of $\Pi(\mathbf{s} \mid \mathbf{X})$, the credible ball is effectively a central region of the posterior distribution for \mathbf{s} . In light of these measures for expressing uncertainty under Binder’s and the VI loss, we propose analogs of credible balls and the PSM that are unique to FOLD.

We focus on the clustering that minimizes (2),

$$\mathbf{c}_{\mathcal{G}} = \underset{\hat{\mathbf{c}}}{\operatorname{argmin}} \mathcal{L}_g(\hat{\mathbf{c}}, \mathbf{s}; \boldsymbol{\theta}). \quad (8)$$

In Proposition 1, we showed that $\mathbf{c}_{\mathcal{G}}$ is only equal to \mathbf{s} if the entries of $\boldsymbol{\theta}$ are perfectly separated via the Hellinger distance. An implication of (8) is that $\mathbf{c}_{\mathcal{G}}$ depends on ω , while the component labels clearly do not. To see this, we recall (5), which shows that we can acquire a clustering with loss smaller than \mathbf{s} by merging any two components with Hellinger distance below γ . Thus, we formulate our measures of uncertainty with respect to the FOLD posterior $\Pi(\mathbf{c}_{\mathcal{G}} \mid \mathbf{X})$, instead of $\Pi(\mathbf{s} \mid \mathbf{X})$.

Accordingly, the 95% credible ball around \mathbf{c}_{FOLD} is defined as

$$B_D(\mathbf{c}_{\text{FOLD}}) = \{\mathbf{c} : D(\mathbf{c}_{\text{FOLD}}, \mathbf{c}) \leq \epsilon_{\text{FOLD}}\}$$

where $\epsilon_{\text{FOLD}} \geq 0$ is the smallest radius such that $\Pi\{D(\mathbf{c}_{\text{FOLD}}, \mathbf{c}_{\mathcal{G}}) \leq \epsilon_{\text{FOLD}} \mid \mathbf{X}\} \geq 0.95$. We interpret $B_D(\mathbf{c}_{\text{FOLD}})$ as a neighbourhood of clusterings centred at our Bayes estimator with posterior probability mass of at least 0.95. Larger ϵ_{FOLD} means that the FOLD posterior

distributes its mass across a larger set around \mathbf{c}_{FOLD} , implying that we are more uncertain about the cluster allocations of the point estimator. In practice, we characterize the credible ball with bounds that give a sense of the clusterings contained within it (Wade and Ghahramani, 2018), much like we would for an interval on the real line. The horizontal bounds of the credible ball consist of the clusterings $\mathbf{c} \in B_D(\mathbf{c}_{\text{FOLD}})$ for which $D(\cdot, \mathbf{c}_{\text{FOLD}})$ attains its maximum value. We can also impose further restrictions on our bounds, such as requiring that they contain the minimum or maximum number of clusters over $B_D(\mathbf{c}_{\text{FOLD}})$ while also maximizing $D(\cdot, \mathbf{c}_{\text{FOLD}})$ amongst groupings with the same number of clusters, giving rise to the notions of vertical upper and vertical lower bounds, respectively.

Figure 3 shows the 95% credible ball of a clustering point estimator calculated using the same location Gaussian mixture fit in Figure 2. Here, we set $\omega = 118.2$, leading to three clusters in the point estimator. The bounds of the credible ball convey our uncertainty in \mathbf{c}_{FOLD} , particularly in the region of the sample space where the tips of the crescents are closest to each other. The vertical lower bound communicates that this region could be split into multiple clusters, while the horizontal and vertical upper bound meld two of the clusters in \mathbf{c}_{FOLD} , corresponding exactly to the crescents.

Alternatively, one can display the PSM for $\mathbf{c}_{\mathcal{G}}$, $\mathcal{P} = \{\Pi(c_{i\mathcal{G}} = c_{j\mathcal{G}} \mid \mathbf{X})\}_{i,j}$, as a heatmap, with the entries ordered by \mathbf{c}_{FOLD} . In general, $\mathcal{P} \neq P$, further demonstrating the distinction between $\Pi(\mathbf{c}_{\mathcal{G}} \mid \mathbf{X})$ and $\Pi(\mathbf{s} \mid \mathbf{X})$. \mathcal{P} is useful for visualization, as the uncertainty in allocating two observations to the same or different cluster is given directly by inspection of the FOLD posterior.

2.4 Implementation with MCMC Output

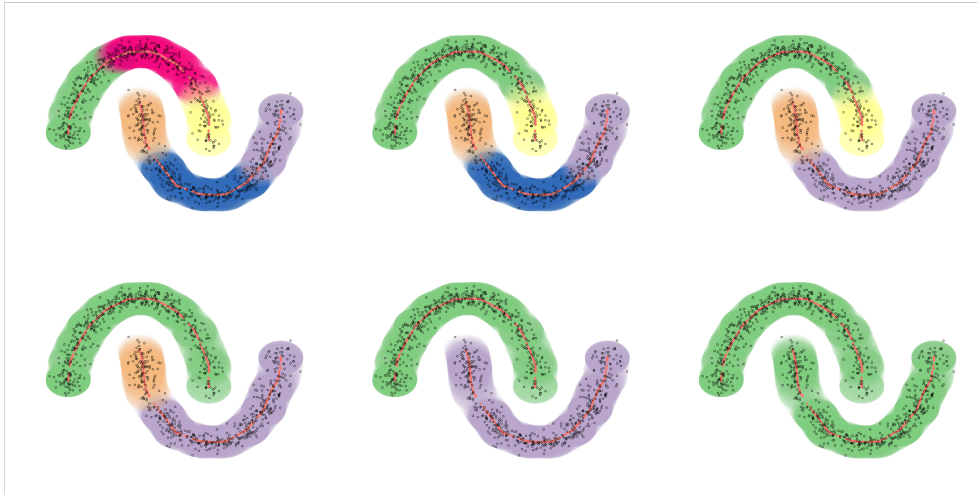


Figure 4: Candidate clusterings of the moons data under a location Gaussian mixture model, generated from average linkage hierarchical clustering on Δ .

Generally, $\Pi(\mathbf{s}, \boldsymbol{\theta} \mid \mathbf{X})$ will not be available in closed form, so Markov chain Monte Carlo (MCMC) algorithms are used to generate posterior samples $\mathbf{s}^{(t)}$ and $\boldsymbol{\theta}^{(t)}$ for $t = 1, \dots, T$ iterations. There is a vast literature proposing a rich variety of MCMC algorithms for mixture models ranging from mixtures of finite mixtures (Miller and Harrison, 2018) to

models allowing infinitely many components, such as Dirichlet process mixtures (Neal, 2000; Jain and Neal, 2004, 2007) and Pitman-Yor process mixtures (Ishwaran and James, 2001, 2003).

The FOLD methodology relies on samples from $\Pi(\mathbf{s}, \boldsymbol{\theta} \mid \mathbf{X})$, which are used to estimate pairwise Hellinger distances,

$$\Delta_{ij} \approx \frac{1}{T} \sum_{t=1}^T \mathcal{H}_{ij}^{(t)}, \quad (9)$$

where $\mathcal{H}_{ij}^{(t)} = h \left\{ g(\theta_{s_i}^{(t)}), g(\theta_{s_j}^{(t)}) \right\}$, and $\theta_{s_i}^{(t)}, \theta_{s_j}^{(t)}$ are computed directly from $\mathbf{s}^{(t)}$ and $\boldsymbol{\theta}^{(t)}$. For many families of kernels, such as the Gaussian family, $h \left\{ g(\theta_{s_i}), g(\theta_{s_j}) \right\}$ is available in closed form. The label-switching problem, which results from the inherent non-identifiability of mixture models with any permutation of the labels yielding the same likelihood (Redner and Walker, 1984), has no impact on FOLD as Δ_{ij} is invariant to labeling. FOLD can be easily applied to virtually any mixture model for which samples from $\Pi(\mathbf{s}, \boldsymbol{\theta} \mid \mathbf{X})$ can be obtained and Hellinger distances between kernels can be estimated.

In practice, \mathbf{c}_{FOLD} is obtained by minimizing (6) over a tree of clusterings produced by average linkage hierarchical clustering on Δ . This procedure is motivated by the appearance of average linkage as a criterion for merging clusters in (5). Figure 4 displays several clusterings of the moons data that result from average linkage clustering on Δ . The true grouping of the data is present amongst the candidates. Since these groupings are hierarchical, Figure 4 can be interpreted as an enumeration of clusterings favoured by $\mathcal{R}_{\mathcal{G}}(\hat{\mathbf{c}} \mid \mathbf{X})$, arranged by increasing values of ω . A similar method with single-linkage is defined in Aragam et al. (2020), and Medvedovic and Sivaganesan (2002) and Fritsch and Ickstadt (2009) also use hierarchical clustering to approximately minimize clustering loss functions. Recent Bayesian clustering algorithms for minimizing loss functions, such as SALSO (Dahl et al., 2020), can also be applied to FOLD.

To express uncertainty in \mathbf{c}_{FOLD} , we rely on samples from $\Pi(\mathbf{c}_{\mathcal{G}} \mid \mathbf{X})$. Given $\mathbf{s}^{(t)}$ and $\boldsymbol{\theta}^{(t)}$, FOLD generates an approximate sample $\mathbf{c}_{\mathcal{G}}^{(t)}$ with

$$\mathbf{c}_{\mathcal{G}}^{(t)} = \operatorname{argmin}_{\hat{\mathbf{c}} \in \mathcal{C}(\mathcal{H}^{(t)})} \sum_{i < j} \left\{ \mathbf{1}_{\hat{c}_i = \hat{c}_j} \mathcal{H}_{ij}^{(t)} + \omega \mathbf{1}_{\hat{c}_i \neq \hat{c}_j} \left(1 - \mathcal{H}_{ij}^{(t)} \right) \right\}, \quad (10)$$

where $\mathcal{C}(\mathcal{H}^{(t)})$ is a list of clusterings generated by average-linkage clustering on $\mathcal{H}^{(t)} = (\mathcal{H}_{ij}^{(t)})_{i,j}$. Using these samples, $B_D(\mathbf{c}_{\text{FOLD}})$ and \mathcal{P} can be estimated. The posterior probability of a credible ball of radius ϵ is approximated by

$$\Pi \{ D(\mathbf{c}_{\mathcal{G}}, \mathbf{c}_{\text{FOLD}}) \leq \epsilon \mid \mathbf{X} \} \approx \frac{1}{T} \sum_{t=1}^T \mathbf{1}_{D(\mathbf{c}_{\mathcal{G}}^{(t)}, \mathbf{c}_{\text{FOLD}}) \leq \epsilon}, \quad (11)$$

and FOLD computes ϵ_{FOLD} by incrementally increasing the value of ϵ over a grid. The entries of \mathcal{P} are estimated via

$$\mathcal{P}_{ij} = \Pi(c_{i\mathcal{G}} = c_{j\mathcal{G}} \mid \mathbf{X}) \approx \frac{1}{T} \sum_{t=1}^T \mathbf{1}_{c_{i\mathcal{G}}^{(t)} = c_{j\mathcal{G}}^{(t)}}. \quad (12)$$

To ensure efficient computation, the 95% credible ball around \mathbf{c}_{FOLD} and posterior similarity matrix are obtained by applying the corresponding R functions in `mcclust.ext` (Wade and Ghahramani, 2018) and `mcclust` (Fritsch, 2022), respectively, to these samples. FOLD summarizes the credible ball by supplying the user with the vertical and horizontal bounds of $B_D(\mathbf{c}_{\text{FOLD}})$, which can then be plotted in the same manner as Figure 3. $D(\cdot, \cdot)$ can be set to either the VI loss or Binder’s loss, with VI as the default.

The loss parameter ω controls the separation among the inferred clusters, and impacts not only \mathbf{c}_{FOLD} but also $B_D(\mathbf{c}_{\text{FOLD}})$ and \mathcal{P} . Similarly to common practice in choosing key tuning parameters in other loss-based clustering contexts, we rely on an elbow plot diagnostic. At a grid of possible ω values, we calculate

$$r_\omega = \frac{\sum_{h=1}^{K_\omega} \sum_{i,j \in C_{\omega,h}} \Delta_{ij}}{\sum_{i < j} \Delta_{ij}}, \quad (13)$$

where $C_{\omega,h}$ is the h th cluster and K_ω is the number of clusters in the minimizer of (6). The numerator in (13) estimates the total within-cluster Hellinger distance between localized densities for a particular ω ,

$$\sum_{h=1}^{K_\omega} \sum_{i,j \in C_{\omega,h}} \mathcal{H}_{ij} = \sum_{i < j} \mathcal{H}_{ij} - \sum_{h < k} \sum_{\substack{i \in C_{\omega,h} \\ j \in C_{\omega,k}}} \mathcal{H}_{ij}, \quad (14)$$

and the denominator normalizes so that $r_\omega \in [0, 1]$ for all ω .

Observe that $r_0 = 0$, $r_\infty = 1$, and r_ω is an increasing function of ω . Since we optimize (7) over a set of candidate groupings produced by hierarchical clustering, as ω increases clusters will gradually be merged together. The value r_ω can be interpreted as the normalized Hellinger cost of pooling two candidate clusters together. For small ω , observations whose localized densities are largely overlapping will be allocated to the same group. However, as ω increases, eventually observations with limited overlap in their localized densities will be clustered together, leading to a sharp increase in the within-cluster Hellinger distance. We propose to increment ω until this threshold is reached, and then choose the clustering at the r_ω threshold.

Alternatively, one can use the default value $\omega^{\text{AVG}} = \gamma^{\text{AVG}} / (1 - \gamma^{\text{AVG}})$, with $\gamma^{\text{AVG}} = \frac{2}{n(n-1)} \sum_{i < j} \Delta_{ij}$. Under this choice of ω , candidate clusters are combined when the average of Δ_{ij} between the clusters is smaller than the average of Δ_{ij} across the entire sample. γ^{AVG} estimates a weighted sum of the total pairwise Hellinger distances between the kernels in f ,

$$\bar{\mathcal{H}} = \frac{1}{\binom{n}{2}} \sum_{i < j} \mathcal{H}_{ij} = \sum_{l < m} \frac{|S_l| |S_m|}{\binom{n}{2}} h \{g(\theta_l), g(\theta_m)\}. \quad (15)$$

Each component is weighted by the number of observations that are allocated to it by \mathbf{s} . If we use $\bar{\mathcal{H}} / (1 - \bar{\mathcal{H}})$ in place of ω in (2), (5) implies that FOLD will favour merging mixture components when $h \{g(\theta_l), g(\theta_m)\} < \bar{\mathcal{H}}$. Importantly, the decision to merge components will depend on how separated they are from the others, as well as the number of observations assigned to each component. To see this, consider the following example, in which we

fit a mixture with $L = 3$ components, where $h\{g(\theta_1), g(\theta_2)\} = \epsilon > 0$, $h\{g(\theta_1), g(\theta_3)\} = h\{g(\theta_2), g(\theta_3)\} = \delta > 0$, and $|S_1| = |S_2| = |S_3| = n/3$. Then, as n grows large, $\mathcal{H} \rightarrow (2/9)\epsilon + (4/9)\delta$, and so FOLD will favour merging S_1 and S_2 into one cluster when $\epsilon < \frac{4}{7}\delta$. The smaller δ is, the smaller ϵ must be in order to merge S_1 and S_2 . Hence, ω^{AVG} excels at problems in which f_0 is composed of well-separated kernels that are approximated by multiple components in f . We show that ω^{AVG} performs very well in this setting in Section 4.

3 Asymptotic Analysis

Most of the study of large sample properties of Bayesian clustering has assumed the kernel is correctly specified, though even in that case problems can result in using infinite mixtures when the truth is finite (Miller and Harrison, 2013, 2014; Cai et al., 2021). Results on the posterior contraction behaviour of the mixing measure (Nguyen, 2013; Ho and Nguyen, 2016b; Guha et al., 2021) provide valuable insight into the large sample behaviour of FOLD. This is because the posterior distribution of the localized densities depends heavily on the mixing measure, which can be deduced by integrating over λ ,

$$\Pi(\theta_{s_i} | \mathbf{X}) = \int_{\lambda} \frac{\lambda(\theta_{s_i})g(X_i; \theta_{s_i})}{f^{(\lambda)}(X_i)} d\Pi(\lambda | \mathbf{X}). \quad (16)$$

We will show that concentration of λ causes Δ to approach optimal values in misspecified regimes. Before we discuss this in full, we briefly summarize the conditions for our analysis. We collect all formal assumptions and proofs for our asymptotic results in the Supplementary Material, which also contains theoretical support for FOLD in the well-specified kernel case.

3.1 General Assumptions

We assume the model satisfies some standard requirements: the parameter space $\Theta \subset \mathbb{R}^d$ must be a compact set and $f^{(\lambda)}$ must be identifiable with respect to the mixing measure, that is, $f^{(\lambda_1)} = f^{(\lambda_2)}$ if and only if $\lambda_1 = \lambda_2$. Identifiability of the mixing measure is satisfied by location and location-scale GMMs, as well as various exponential family mixtures (Barndorff-Nielsen, 1965) and location family mixtures (Teicher, 1961). We opt for simplicity by focusing on overfitted mixtures that fix $L < \infty$ and choose $\Pi(\mathbf{a})$ as a symmetric Dirichlet prior with concentration parameter $0 < \alpha < 1$. In addition, we assume the prior $\Pi(\theta_l)$ is absolutely continuous and with full support on Θ .

We assume second-order identifiability of the kernel family \mathcal{G} (Ho and Nguyen, 2016b), requiring the density function and the first and second derivatives of $g(x; \theta)$ with respect to θ to be linearly independent. The location Gaussian family and certain other location families are second-order identifiable (Chen, 1995; Manole and Ho, 2022), but the location-scale Gaussian family is not (Ho and Nguyen, 2016b). For continuity, we will require the second derivatives of $g(x; \theta)$ satisfy an integral Lipschitz condition in θ with respect to f_0 , as in Guha et al. (2021), which can be satisfied for location-Gaussians (Ho et al., 2020). These identifiability and continuity conditions will be useful for posterior contraction of λ .

3.2 KL-Oracle Concentration

When f_0 is not a mixture over \mathcal{G} the posterior may assign samples to an exorbitant number of components as the sample size grows. To study this behaviour, we examine posterior contraction of the mixing measure. Guha et al. (2021) showed that λ contracts in the 2-Wasserstein metric to the Kullback-Leibler (KL) divergence minimizer,

$$\lambda^* = \operatorname{argmin}_{\lambda \in \Omega(\Theta)} \operatorname{KL}(f_0, f^{(\lambda)}), \quad (17)$$

where $\Omega(\Theta)$ is the set of all probability measures on Θ . We assume that λ^* exists, is unique, and has finite support, with $\lambda^* = \sum_{k=1}^{K^*} a_k^* \delta_{\theta_k^*}$ and $f^* = f^{(\lambda^*)} = \sum_{k=1}^{K^*} a_k^* g(\theta_k^*)$ for some $K^* < L$. Depending on the degree of misspecification, K^* can be very large, making the component labels impractical for cluster analysis. Contraction of λ implies the following concentration behaviour for the weights and atoms.

Proposition 3. Let $\epsilon_n = (\log n/n)^{1/4}$, $0 < \delta < 1$, and $R^* = L - K^*$. For any $h \in [K^*]$ and $\mathcal{I} \subset [L]$, define the events

$$A_{h,\mathcal{I}} = \left\{ \max_{l \in \mathcal{I}} \|\theta_l - \theta_h^*\| \lesssim \epsilon_n, \left| \sum_{l \in \mathcal{I}} a_l - a_h^* \right| \lesssim (\epsilon_n \vee \epsilon_n^{2\delta}) \right\},$$

$$B_{\mathcal{I}} = \left\{ \sum_{l \in \mathcal{I}} a_l \lesssim \epsilon_n^{2\delta} \right\}.$$

Then under conditions (A1)-(A4), as $n \rightarrow \infty$,

$$\mathbb{E}_0 \left[\Pi \left\{ \left(\bigcap_{h=1}^{K^*} \bigcup_{|\mathcal{I}| \geq 1} A_{h,\mathcal{I}} \right) \cap \left(\bigcup_{|\mathcal{I}| \leq R^*} B_{\mathcal{I}} \right) \mid \mathbf{X} \right\} \right] \rightarrow 1. \quad (18)$$

Proposition 3 provides the following conclusion on the limiting values of the atoms and weights as λ contracts to λ^* . For any component k of λ^* , there exists a subset of components in λ so that each atom is within an ϵ_n neighbourhood of θ_k^* , and the cumulative weight of that subset is within a $\max(\epsilon_n, \epsilon_n^{2\delta})$ neighbourhood of a_h^* . Any other components in λ have total weight that diminishes at a rate of $\epsilon_n^{2\delta}$. (18) highlights that both the atoms and weights are useful in merging mixture components, as there is no guarantee on the asymptotic behaviour of atoms in λ that are not within ϵ_n neighbourhoods of the atoms of λ^* . Conveniently, these potentially problematic components are made redundant by their diminishing weight. The behaviour of the components in (18) is a direct consequence of 2-Wasserstein concentration in λ , and has been exploited for mixing measure estimation in well-specified regimes in the Merge-Truncate-Merge algorithm (Guha et al., 2021).

Proposition 3 can be used to show that Δ will concentrate on optimal values with respect to our model class. We define the KL-oracle clustering as \mathbf{c}_{FOLD} when λ^* and f^* are known,

$$\mathbf{c}_{\text{FOLD}}^{\text{KL}} = \operatorname{argmin}_{\hat{\mathbf{c}}} \sum_{i < j} \{ \mathbf{1}_{\hat{c}_i = \hat{c}_j} \Delta_{ij}^* + \omega \mathbf{1}_{\hat{c}_i \neq \hat{c}_j} (1 - \Delta_{ij}^*) \}, \quad (19)$$

where Δ^* has entries $\Delta_{ij}^* = \mathbb{E}_\Pi(\mathcal{H}_{ij} \mid \lambda^*, \mathbf{X}) = \sum_{k < h} h \{g(\theta_k^*), g(\theta_h^*)\} q_{ij}^{kh*}$,

$$q_{ij}^{kh*} = \Pi\{(s_i, s_j \in S_k \cup S_h) \cap (s_i \neq s_j) \mid \mathbf{X}, \lambda^*\}.$$

As n grows arbitrarily large, the cluster allocations in \mathbf{c}_{FOLD} and $\mathbf{c}_{\text{FOLD}}^{\text{KL}}$ coincide. This limiting behaviour follows directly from (18), as concentration of $\boldsymbol{\theta}$ and \mathbf{a} can be used to show that Δ_{ij} and Δ_{ij}^* become arbitrarily close.

In order to prove this formally, we need to make two further assumptions on \mathcal{G} . First, we assume that \mathcal{G} is a location family, i.e., $g(x; \theta) = \tilde{g}(x - \theta)$ for some probability density function \tilde{g} . Second, we require that $\tilde{g}(z)$ is ζ -Hölder continuous for some $\zeta > 0$. It can be verified that location Gaussian kernels satisfy these assumptions with $\zeta = 1$.

Theorem 1. Let $\epsilon_n = (\log n/n)^{1/4}$, $0 < \delta < 1$, and assume conditions (A1)-(A6). Then, for all $n \geq N$ for some $N \in \mathbb{N}$ and each pair of observations $i < j$, there exists a constant $M > 0$ and random variables $\Delta_{ij}^{*-} = \Delta_{ij}^* - o_{\mathbb{P}_0}(1)$ and

$$\Delta_{ij}^{*+} = \Delta_{ij}^* + o_{\mathbb{P}_0}(1) + \frac{M \left\{ \binom{L}{2} - \binom{K^*}{2} \right\} \epsilon_n^{2\delta}}{f^*(X_i)f^*(X_j) - o_{\mathbb{P}_0}(1)} \quad (20)$$

so that with \mathbb{P}_0 -probability equal to 1,

$$\Delta_{ij}^{*-}(1 - o_{\mathbb{P}_0}(1)) + o_{\mathbb{P}_0}(1) \leq \Delta_{ij} \leq \Delta_{ij}^{*+}(1 - o_{\mathbb{P}_0}(1)) + o_{\mathbb{P}_0}(1). \quad (21)$$

Pragmatically, Proposition 3 and Theorem 1 give a concrete notion of the limiting values of \mathbf{c}_{FOLD} . As we observe more data, minimizing (6) becomes equivalent to the KL-oracle clustering, in which we group observations generated from f_0 using our knowledge of the best approximation f^* to the true state of nature. Also, the tightness of the bounds in (21) provide some understanding of the effects on \mathbf{c}_{FOLD} of overfitting finite mixtures and observing outliers. $|\Delta_{ij}^{*+} - \Delta_{ij}^*|$ is smaller when the remainder term in (20) is small. The larger L is relative to K^* , the larger this remainder becomes. Likewise, observations that are given low density by f^* also blow up $|\Delta_{ij}^{*+} - \Delta_{ij}^*|$. In this case, provided that $\int_{\mathbb{R}^d} \frac{f_0(x)}{f^*(x)} dx < \infty$, the remainder will be small on average as n grows, since

$$\mathbb{E}_0 \left\{ \frac{M \left\{ \binom{L}{2} - \binom{K^*}{2} \right\} \epsilon_n^{2\delta}}{f^*(X_i)f^*(X_j)} \right\} \lesssim (\log n/n)^{\delta/2}. \quad (22)$$

3.3 Location Gaussian Mixtures

When $\mathcal{G} = \{\mathcal{N}_d(\theta, \Sigma) : \theta \in \Theta\}$ for some covariance matrix Σ , the Hellinger distance between the kernels in f^* is directly related to the Mahalanobis distance between their means,

$$1 - h^2 \{g(\theta_k^*), g(\theta_h^*)\} \propto \exp \left(-\frac{1}{8} \mathcal{M}_{kh}^2 \right), \quad (23)$$

$$\mathcal{M}_{kh} = \sqrt{(\theta_k^* - \theta_h^*)^T \Sigma^{-1} (\theta_k^* - \theta_h^*)}. \quad (24)$$

Intuitively, this tells us that in the large sample limit, if two observations are best modeled as being generated from separate components in f^* , FOLD will favour allocating them to the

same cluster when the means of their associated components are close under the Mahalanobis distance. Hence, the role of Σ is very important for merging mixture components. To see this better, consider the case where $\Sigma = \sigma^2 \mathbf{I}_d$. We can rewrite the Mahalanobis distance as a weighted version of the Euclidean norm, $\mathcal{M}_{kj} = \|\theta_k^* - \theta_h^*\| / \sigma$. It follows that

$$\lim_{\sigma \rightarrow 0} \Delta_{ij}^* = \Pi(s_i \neq s_j \mid \mathbf{X}, \lambda^*), \quad \lim_{\sigma \rightarrow \infty} \Delta_{ij}^* = 0. \quad (25)$$

The latter result is expected, as higher variance in the kernels will effectively fit one large Gaussian kernel to the entire dataset. At the other extreme, small variance causes FOLD to converge to KL-oracle values of Binder’s loss. This behaviour is reminiscent of Proposition 1 because the kernels in f^* will be perfectly separated for very small σ .

For applications, we recommend giving Σ a weakly informative prior distribution, allowing the covariance to be informed by the data rather than selected by the user. We also find that location-scale Gaussian mixtures perform well with FOLD, in part due to their added flexibility that generally leads to fewer mixture components. However, as mentioned previously, location-scale Gaussians fail the second-order identifiability requirement of our asymptotic theory. Theoretical guarantees on location-scale Gaussian mixtures and other weakly identifiable mixtures is an open area of research, but recent progress has been made for maximum likelihood estimates (Ho and Nguyen, 2016a; Manole and Ho, 2022).

4 Simulation Studies

In this section, we demonstrate with several numerical examples that FOLD is robust to a diverse range of cluster shapes despite the data being modeled with a Gaussian mixture. Code for the simulated data and computation of \mathbf{c}_{FOLD} is available on the GitHub page of the first author. See the Supplementary Material for further details on all simulations and an additional simulation study focused on credible balls.

4.1 Effect of Increasing n on Model-Based Clustering

	n	FOLD	Oracle FOLD	VI	Binder’s	Mclust
No. of Clusters	100	2.93 (0.383)	3.00 (0.00)	8.02 (5.714)	19.76 (0.818)	3.10 (0.414)
	500	3.06 (0.278)	3.00 (0.00)	3.53 (0.926)	19.89 (0.852)	3.00 (0.00)
	1000	3.05 (0.219)	3.00 (0.00)	3.30 (0.541)	19.96 (0.400)	3.01 (0.100)
	2500	3.05 (0.219)	3.00 (0.00)	3.08 (0.273)	20.00 (0.00)	3.00 (0.00)
Adj. Rand Index	100	0.903 (0.087)	0.985 (0.021)	0.852 (0.088)	0.822 (0.061)	0.962 (0.052)
	500	0.979 (0.013)	0.998 (0.008)	0.974 (0.014)	0.947 (0.012)	0.987 (0.008)
	1000	0.985 (0.006)	0.987 (0.006)	0.982 (0.007)	0.968 (0.007)	0.985 (0.024)
	2500	0.986 (0.004)	0.987 (0.004)	0.984 (0.004)	0.979 (0.005)	0.987 (0.004)

Table 1: Averages and standard deviations (in parentheses) for the number of clusters and adjusted Rand index with \mathbf{s}_0 on 100 replications from a mixture of bivariate Gaussian kernels.

In light of the asymptotic results shown in the previous section, we examine the effect of increasing n on FOLD and other model-based clustering methods. For a given f_0 , we

	n	FOLD	VI	Binder's	Mclust
No. of Clusters	100	3.02 (0.141)	3.16 (0.395)	13.84 (6.080)	3.14 (0.377)
	500	3.03 (0.171)	3.42 (0.755)	6.15 (2.258)	3.23 (0.529)
	1000	3.20 (0.449)	3.53 (0.881)	9.32 (3.816)	4.33 (1.429)
	2500	3.19 (0.443)	3.40 (0.682)	8.93 (2.409)	7.99 (0.959)
Adj. Rand Index	100	0.992 (0.016)	0.987 (0.021)	0.915 (0.043)	0.989 (0.030)
	500	0.999 (0.003)	0.998 (0.003)	0.992 (0.006)	0.980 (0.049)
	1000	0.999 (0.002)	0.997 (0.007)	0.990 (0.009)	0.866 (0.149)
	2500	0.999 (0.001)	0.990 (0.020)	0.952 (0.014)	0.576 (0.071)

Table 2: Averages and standard deviations (in parentheses) for the number of clusters and adjusted Rand index with \mathbf{s}_0 on 100 replications from a mixture of bivariate skew Gaussian kernels.

	n	FOLD	VI	Binder's	Mclust
No. of Clusters	100	3.25 (0.500)	3.89 (1.014)	12.62 (4.292)	3.56 (0.925)
	500	3.23 (0.601)	3.64 (0.894)	13.94 (4.552)	4.17 (0.779)
	1000	3.10 (0.302)	4.83 (1.025)	15.73 (3.795)	5.08 (0.442)
	2500	3.10 (0.302)	4.58 (0.843)	18.99 (2.634)	6.20 (0.876)
Adj. Rand Index	100	0.982 (0.029)	0.974 (0.026)	0.800 (0.094)	0.884 (0.177)
	500	0.995 (0.032)	0.921 (0.136)	0.799 (0.147)	0.715 (0.159)
	1000	0.975 (0.085)	0.691 (0.057)	0.665 (0.037)	0.574 (0.054)
	2500	0.967 (0.098)	0.679 (0.012)	0.639 (0.027)	0.512 (0.056)

Table 3: Averages and standard deviations (in parentheses) for the number of clusters and adjusted Rand index with \mathbf{s}_0 on 100 replications from the skew-symmetric mixture.

repeatedly simulate observations with varying $n \in \{100, 500, 1000, 2500\}$ for 100 replications each. We compare FOLD with $\omega = \omega^{\text{AVG}}$ to clusterings returned by minimizing Binder's loss and the VI loss using the packages `mclust` and `mclust.ext`, respectively. Along with these Bayesian approaches, we also cluster the data using `mclust` (Scrucca et al., 2016), which groups observations based on the EM algorithm for a Gaussian mixture.

For each replication and n , we run the EM algorithm and fit a Bayesian location-scale GMM,

$$X_i \mid \mathbf{a}, \boldsymbol{\mu}, \boldsymbol{\Sigma} \sim \sum_{l=1}^L a_l \mathcal{N}_2(\mu_l, \Sigma_l); \quad (26)$$

$$(\mu_l, \Sigma_l) \sim \mathcal{N} - \mathcal{IW}(\mu, \kappa, \nu, \Psi), \quad l = 1, \dots, L; \quad (27)$$

$$\mathbf{a} \sim \text{Dirichlet}((\alpha, \dots, \alpha)). \quad (28)$$

We then compute clusterings with FOLD, VI, and Binder's loss using the posterior samples from the Bayesian model. For each clustering, we save the number of clusters and the adjusted Rand index (Rand, 1971) with \mathbf{s}_0 . The hyperparameters are set at $L = 30$, $\alpha = 1/2$, and $\boldsymbol{\mu} = \mathbf{0}_d$, $\kappa = 1$, $\nu = d + 2$, and $\boldsymbol{\Psi} = \mathbf{I}_d$. We run a Gibbs sampler for 9,000 iterations with a burn-in of 1,000, then use every third iteration for computing the Bayesian clusterings. For `mclust`, the number of clusters is automatically selected each replication by minimizing the Bayesian information criterion (BIC).

In the first scenario, we let $f_0(x) = \sum_{k=1}^3 \pi_{0k} \mathcal{N}_2(x; \mu_{0k}, \Sigma_{0k})$, with weights $\boldsymbol{\pi}_0 = (0.45, 0.25, 0.3)$

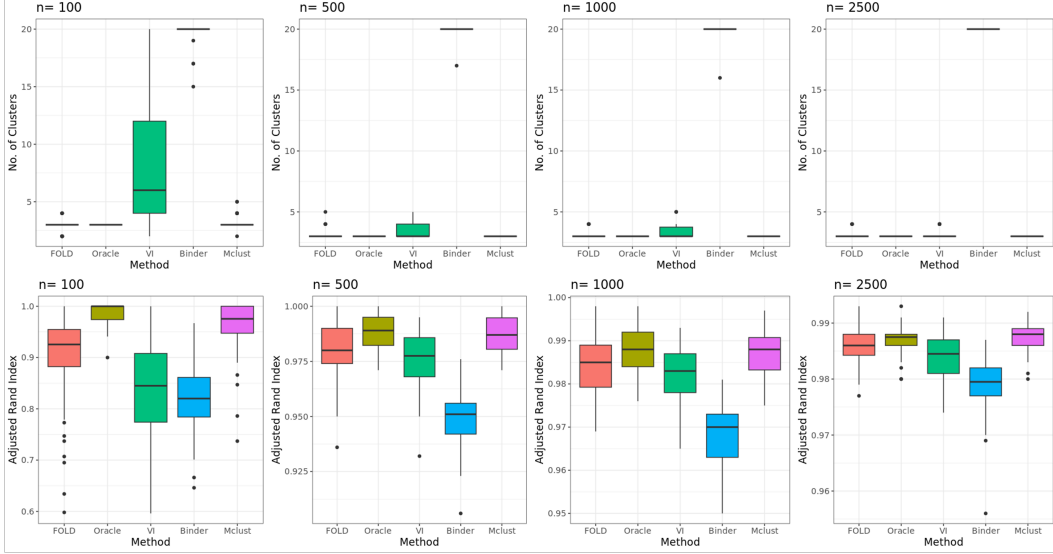


Figure 5: Comparison of the number of clusters and the adjusted Rand index with \mathbf{s}_0 on 100 replications from a mixture of well-separated multivariate Gaussian kernels.

and atoms $\mu_{01} = (6.5, 5)$, $\Sigma_{01} = \mathbf{I}_2$, $\mu_{02} = (0, 0)$, $\Sigma_{02} = \text{diag}(5, 2)$, and $\mu_{03} = (-5, -5)$, $\Sigma_{03} = \text{diag}(3, 1)$. As shown in Figure 11(a) in the Supplementary Material, the three kernels are well separated. Since the data generating process is a Gaussian mixture, we have access to the oracle FOLD clusters,

$$\mathbf{c}_{\text{FOLD}}^{\text{oracle}} = \underset{\hat{\mathbf{c}}}{\text{argmin}} \sum_{i < j} \{ \mathbf{1}_{\hat{c}_i = \hat{c}_j} \Delta_{ij}^0 + \omega \mathbf{1}_{\hat{c}_i \neq \hat{c}_j} (1 - \Delta_{ij}^0) \}, \quad (29)$$

with $\Delta_{ij}^0 = \mathbb{E}_{\Pi}(\mathcal{H}_{ij} \mid \mathbf{X}, \lambda_0)$ and $\omega = \omega^{\text{AVG}}$. Similar to the KL-oracle in misspecified regimes, we expect \mathbf{c}_{FOLD} and $\mathbf{c}_{\text{FOLD}}^{\text{oracle}}$ to become increasingly similar as n grows due to posterior contraction of λ (Nguyen, 2013; Guha et al., 2021). The averages and standard deviations for the number of clusters and adjusted Rand index are given in Table 1, with boxplots of these benchmarks displayed in Figure 5. FOLD, oracle FOLD, and mclust achieve high adjusted Rand index with increasing sample size. Oracle FOLD is perfect at computing the true number of clusters, and mclust and FOLD are also excellent. Furthermore, the number of clusters and adjusted Rand index for \mathbf{c}_{FOLD} gradually approach the values produced by $\mathbf{c}_{\text{FOLD}}^{\text{oracle}}$. The VI loss improves in the number of clusters as n increases, but Binder’s loss falls short, consistently producing 20 clusters with diminishing variation across replications. VI and Binder’s loss produce high adjusted Rand indices that improve with n .

Next, we let $f_0(x) = \sum_{k=1}^3 \pi_{0k} \mathcal{SN}_2(x; \mu_{0k}, \Sigma_{0k}, \psi_{0k})$, where $\mathcal{SN}_2(x; \cdot, \cdot, \cdot)$ denotes the PDF of a bivariate skew Gaussian distribution (Azzalini and Valle, 1996; Azzalini and Capitanio, 1999) and $\boldsymbol{\pi}_0 = (0.45, 0.25, 0.3)$. These kernels have the same location and scale parameters as the bivariate Gaussian mixture in simulation case 1, and skewness parameters $\psi_{01} = (1, 1)$, $\psi_{02} = (-10, 15)$, and $\psi_{03} = (4, -17)$. Figure 11(b) in the Supplementary Material shows a contour plot of f_0 . Results across the replications are reported in Figure 7 and Table 2. For all values of n , FOLD attains high accuracy with a small number of clusters. As n increases, all four clustering methods achieve high levels of the adjusted Rand index, though FOLD

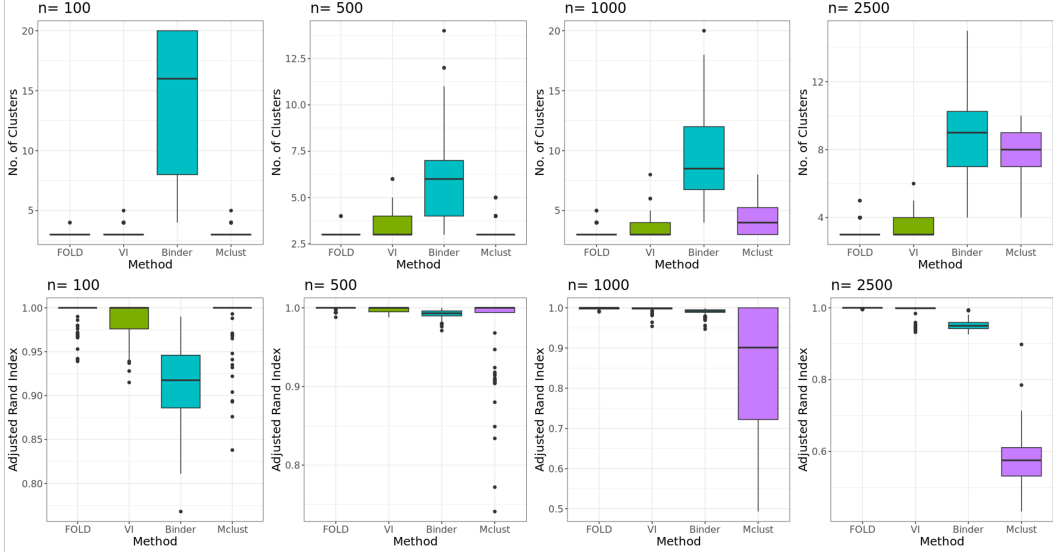


Figure 6: Comparison of the number of clusters and the adjusted Rand index with \mathbf{s}_0 on 100 replications from a mixture of multivariate skew Gaussian distributions.

results in values close to 1 while the VI loss and Binder’s loss decline slightly. FOLD tends to produce between 3 and 4 clusters for each n and reports less than or equal to the number of clusters induced by the VI loss in 94.5% of all instances.

In the final simulation case, we take f_0 to be a bivariate mixture of three kernels with weights $\boldsymbol{\pi}_0 = (0.55, 0.3, 0.15)$. τ_{01} is a mixture of one skew Gaussian kernel and two Gaussian kernels, τ_{02} is a skew Gaussian kernel, and τ_{03} is a Gaussian kernel. We refer to f_0 in this case as a skew-symmetric mixture. As can be seen in Figure 11(c) in the Supplementary, τ_{01} is a non-Gaussian, multimodal density. Similarly, data generated from τ_{02} , the oblong kernel in the lower third of the sample space, will most likely be approximated by multiple components, despite only constituting one cluster. The results of the simulations are summarized in Table 3 and Figure 6. FOLD generally allocates observations to 3 clusters, but the VI loss favours between 3 and 6 clusters. In 96.5% of the replicates, the number of clusters for FOLD is less than or equal to the number for VI. As in simulation case 2, Binder’s loss and `mclust` frequently return a larger number of clusters than the truth for larger n . The adjusted Rand index between \mathbf{c}_{FOLD} and \mathbf{s}_0 is close to 1 across all sample sizes. In contrast, the three other methods achieve high adjusted Rand index for small n , but these values sharply drop for $n \geq 1000$. This is usually the result of splitting τ_{01} or τ_{02} into multiple clusters.

5 Example: GSE81861 Cell Line Dataset

We apply FOLD to the GSE81861 cell line dataset (Li et al., 2017), which measures single cell counts in 57,241 genes from 630 single-cell transcriptomes. There are 7 distinct cell lines present in the dataset, so we compare FOLD and other model-based clustering methods to the true cell line labels as a performance benchmark. We first discard cells with low read counts, giving $n = 519$ total cells. We then normalize the data using SCRAN (Lun et al., 2016) and select informative genes with M3Drop (Andrews and Hemberg, 2019). We

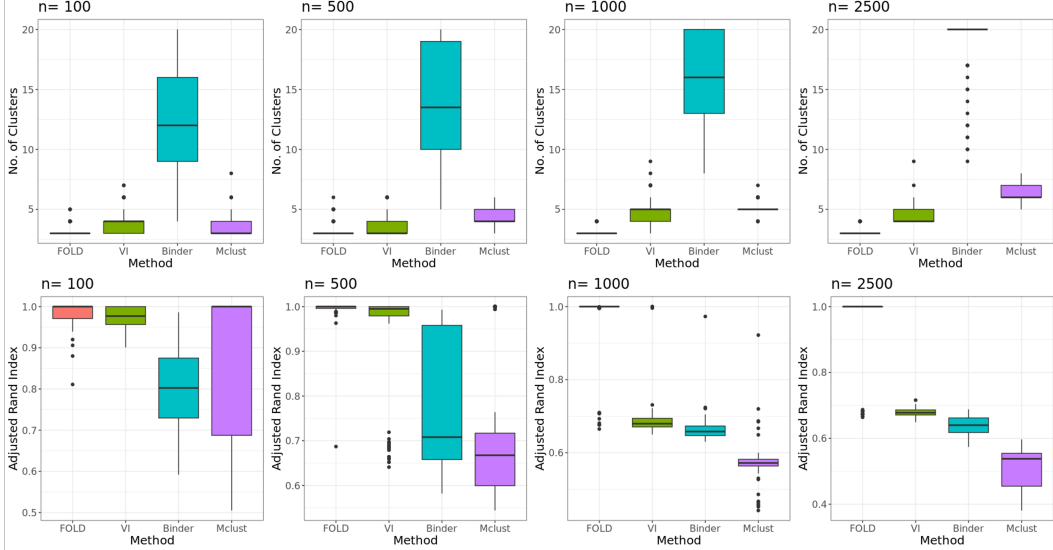


Figure 7: Comparison of the number of clusters and the adjusted Rand index with \mathbf{s}_0 on 100 replications from the skew-symmetric mixture.

use principal component analysis (PCA) for dimension reduction by taking \mathbf{X} to be the projection of the normalized cell counts onto the first $d = 5$ principal components, then scale the projections to have zero mean and unit variance.

We fit a d -dimensional Bayesian location-scale Gaussian mixture to \mathbf{X} with $L = 50$ components, Dirichlet concentration parameter $\alpha = 1/2$, and a Normal-Inverse-Wishart prior with parameters $\mu = 0_d$, $\kappa = 1$, $\nu = d + 2$, and $\Psi = \mathbf{I}_d$. We generate 25,000 posterior samples after a burn-in of 1,000. Every fourth iteration is discarded and we estimate Δ with the remaining 6,000 samples. We choose \mathbf{c}_{FOLD} using an elbow plot, and calculate clusterings with the VI loss and `mclust`. The clusterings of both FOLD and the VI are computed using the same MCMC samples.

For FOLD, we create candidate clusterings by average-linkage clustering on Δ , then choose ω by consulting the elbow plot in Figure 8. The plot suggests 6 clusters, which corresponds to $\omega = 25$. As in our simulations, we choose the number of clusters in `mclust` using BIC. Figure 9 shows the UMAP plots (McInnes et al., 2018) of the original normalized count data along with colours indicating the true cell types and the clusterings from the three methods. The adjusted Rand index with the true cell types for \mathbf{c}_{FOLD} , the VI clusters, and the `mclust` clusters are 0.995, 0.915, and 0.854, respectively. Both the VI loss and `mclust` split the GM12878 cell type into two clusters, though \mathbf{c}_{FOLD} keeps that type as one cluster. Similarly, the H1 cell type is split into multiple clusters by both the VI loss and `mclust`, but kept as a single cluster by \mathbf{c}_{FOLD} . Cluster splitting of the GM12878 and H1 types is expected with this dataset, as these cell types were each sequenced in two separate batches (Li et al., 2017). However, \mathbf{c}_{FOLD} underestimates the number of groups by combining the H1437 and IMR90 cell types. The other methods merge these types as well, with the VI loss producing 9 clusters and `mclust` giving 7 clusters.

We express uncertainty in \mathbf{c}_{FOLD} with a 95% credible ball using $D(\cdot, \cdot)$ as the VI, and display the associated bounds in Figure 10. The credible ball communicates that there is

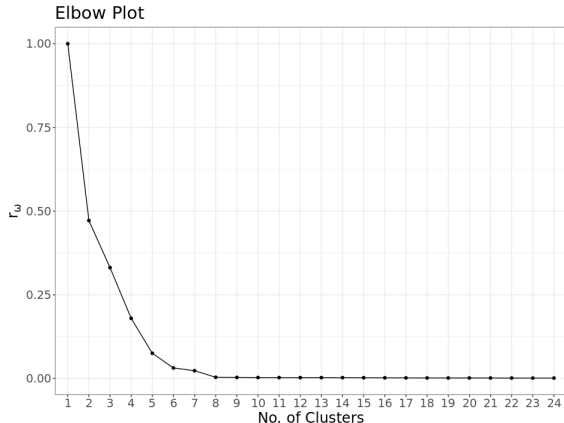


Figure 8: Elbow plot for choosing the number of clusters in \mathbf{c}_{FOLD} with the cell line dataset. We choose 6 clusters, corresponding to $\omega = 25$.

substantial uncertainty in cell types where batch effects occur. The horizontal and vertical upper bounds effectively merge the GM12878 type with the H1437 cell type, which is likely due to the proximity of these two types in the sample space. Conversely, the vertical lower bound splits the GM12878 cell type into two clusters. We are also uncertain in our classification of the H1 cell type, which is similarly split into multiple clusters by the vertical lower bound because of separate batching. Interestingly, in all bounds, the H1437 and IMR90 cell types are allocated to the same cluster. This type merging could be explained by the fact that IMR90 consists of a small number of cells or that both types are isolated from the lung (Li et al., 2017).

6 Discussion

Fusing of Localized Densities (FOLD) is a Bayesian method for cluster analysis that characterizes clusters as possibly containing multiple mixture components. We first detailed the decision theoretic justification behind our approach, in which we obtain a point estimate of the clustering by minimizing a novel loss function. Our loss function has several appealing properties, such as favouring the merging of overlapping kernels, simplification to Binder’s loss when all the mixture components are well separated, and invariance to permutations of the labels. Uncertainty in cluster allocations is expressed with a credible ball and posterior similarity matrix. We have given concrete guidance on tuning the loss parameter, including an elbow plot method and default value that performs excellently on simulated examples.

Throughout the article, we have primarily focused on the Gaussian mixture model because of its ubiquity in the literature and useful theoretical properties. However, FOLD can be applied to any parametric mixture in which the Hellinger distance between kernels is simple to compute, which includes the beta, exponential, gamma, and Weibull families. A near identical approach can be applied to discrete families, where localized mass functions would replace the role of the localized densities.

Building on asymptotic theory from Guha et al. (2021), we have shown that our clustering point estimate is equivalent to a KL-oracle in the large sample limit. Our proof relied on

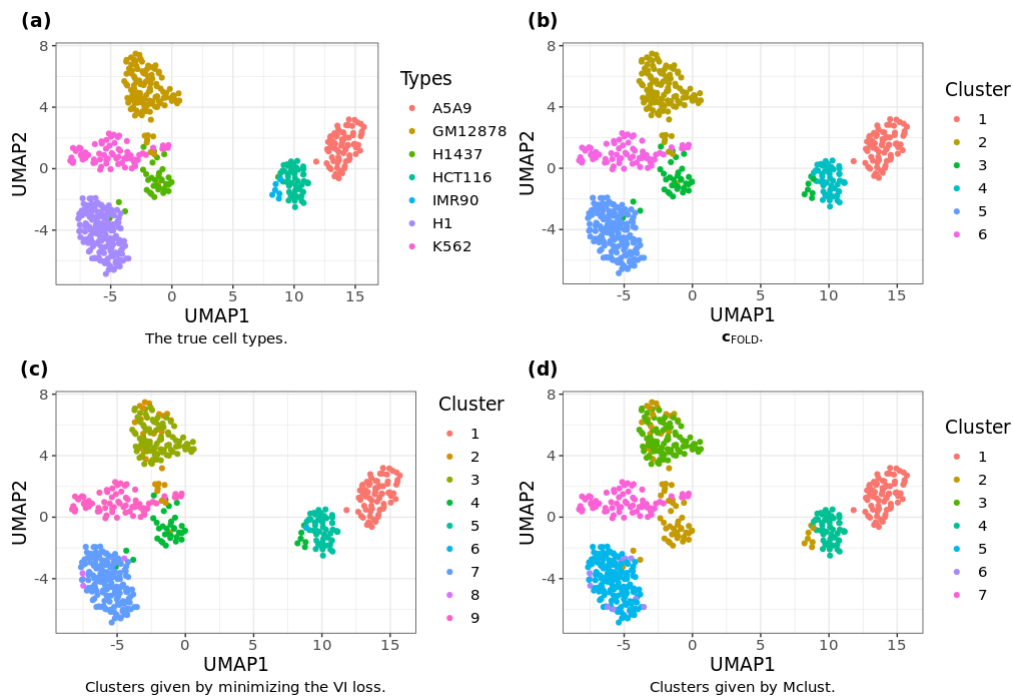


Figure 9: UMAP plots of the cell line dataset with colours corresponding to the true cell types, c_{FOLD} , VI, and $m\text{clust}$, respectively.

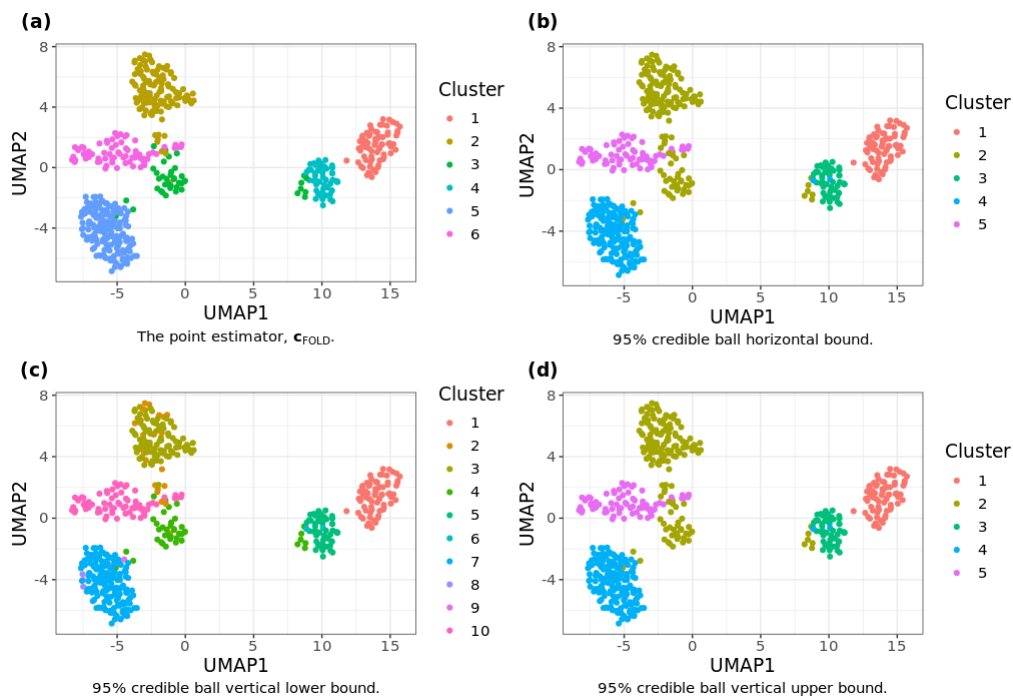


Figure 10: The clustering c_{FOLD} along with the horizontal, vertical lower, and vertical upper bounds for the cell line dataset. Here, $D(\cdot, \cdot)$ is the VI.

consistency of the mixture parameters at the KL-minimizer (Guha et al., 2021). For an overfitted misspecified mixture, a subset of the atoms will concentrate near the atoms of the KL-minimizer, and the remaining atoms will have diminishing weights. This suggests that some of the atoms can be merged together, while other atoms can be discarded.

Though we focused on the Hellinger distance because of its boundedness and simple closed form in many cases, other distribution metrics, such as the total variation distance and the Wasserstein metric, could be used instead. Clusters can be created by treating Δ as a distance matrix and applying k-medoids, hierarchical clustering, or other distance-based methods. An even simpler variant is a distance matrix of the localized atoms θ_{s_i} under an appropriate metric. However, the boundedness of the Hellinger distance is crucial for our loss function, and so deriving the form of a coherent loss for these variants provides an intriguing avenue for future research.

In our theory, we required that the fitted mixture model has a finite number of components, satisfies $L > K^*$, and has kernels belonging to a family that is second-order identifiable. In particular, the latter assumption includes location Gaussian mixtures, but excludes location-scale Gaussian mixtures (Ho and Nguyen, 2016b), though the location-scale family is first-order identifiable. Furthermore, modeling the data with an infinite mixture, in which underfitting the number of components has non-zero mass a priori and the KL-minimizer may have infinite components, would markedly impact the concentration of the entries of Δ . An interesting extension of our results is examining the asymptotic behaviour of FOLD for first-order identifiable families and infinite mixtures.

Appendix A Basic Properties of FOLD

A.1 Proof of Proposition 1

Proof. We proceed as in Dahl et al. (2022) and decompose the loss function into separate terms that relate to the contingency table between $\hat{\mathbf{c}}$ and \mathbf{s} . For any $m, l \in \{1, \dots, L\}$, let $\eta_{ml} = h(g(\theta_m), g(\theta_l))$. For groups \hat{C}_k and S_l , set $n_{k\cdot} = |\hat{C}_k|$, $n_{\cdot l} = |S_l|$, and $n_{kl} = |\hat{C}_k \cap S_l|$.

$$\begin{aligned}
\mathcal{L}_g(\hat{\mathbf{c}}, \mathbf{s}; \boldsymbol{\theta}) &= \sum_{i < j} \{ \mathbf{1}_{\hat{c}_i = \hat{c}_j} \mathcal{H}_{ij} + \omega \mathbf{1}_{\hat{c}_i \neq \hat{c}_j} (1 - \mathcal{H}_{ij}) \} \\
&= \sum_{i < j} \{ \mathbf{1}_{\hat{c}_i = \hat{c}_j} (1 - (1 - \mathcal{H}_{ij})) + \omega (1 - \mathbf{1}_{\hat{c}_i = \hat{c}_j}) (1 - \mathcal{H}_{ij}) \} \\
&= \sum_{i < j} \mathbf{1}(\hat{c}_i = \hat{c}_j) + \omega \sum_{i < j} (1 - \mathcal{H}_{ij}) - (1 + \omega) \sum_{i < j} \mathbf{1}_{\hat{c}_i = \hat{c}_j} (1 - \mathcal{H}_{ij}) \\
&= \sum_{k=1}^{\hat{K}} \binom{n_{k\cdot}}{2} + \omega \sum_{l=1}^L \binom{n_{\cdot l}}{2} + \omega \sum_{m < l} n_{\cdot m} n_{\cdot l} (1 - \eta_{ml}) \\
&\quad - (1 + \omega) \sum_{k=1}^{\hat{K}_n} \sum_{l=1}^L \binom{n_{kl}}{2} - (1 + \omega) \sum_{k=1}^{\hat{K}_n} \sum_{m < l} n_{km} n_{kl} (1 - \eta_{ml}).
\end{aligned}$$

Consequently, this shows that the loss is related to the Binder's loss with unit costs $a = 1$ and $b = \omega$,

$$\mathcal{L}_g(\widehat{\mathbf{c}}, \mathbf{s}; \boldsymbol{\theta}) = \mathcal{L}_B(\widehat{\mathbf{c}}, \mathbf{s}) + \mathcal{B}_g(\widehat{\mathbf{c}}, \mathbf{s}; \boldsymbol{\theta})$$

where

$$\mathcal{B}_g(\widehat{\mathbf{c}}, \mathbf{s}) = \omega \sum_{m < l} n_{\cdot m} n_{\cdot l} (1 - \eta_{ml}) \quad (30)$$

$$- (1 + \omega) \sum_{k=1}^{\hat{K}} \sum_{m < l} n_{km} n_{kl} (1 - \eta_{ml}). \quad (31)$$

It is clear that

$$\mathcal{B}_g(\mathbf{s}, \mathbf{s}) = \omega \sum_{m < l} n_{\cdot m} n_{\cdot l} (1 - \eta_{ml}) \quad (32)$$

which is equal to zero if and only if $\eta_{ml} = 1$ for all m, l pairs. \square

A.2 Proof of Proposition 2

Proof. We proceed by showing that the bounded metric properties of the Hellinger distance are preserved by taking the posterior expectation.

1. For each $i \leq j$, $0 \leq h(g(\theta_{s_i}), g(\theta_{s_j})) \leq 1$ almost surely, and so $0 \leq \Delta_{ij} \leq 1$.
2. We next verify the metric axioms on the entries of Δ .
 - (a) For each $i = 1, \dots, n$, $h(g(\theta_{s_i}), g(\theta_{s_i})) = 0$ almost surely, and so $\Delta_{ii} = 0$.
 - (b) $\Delta_{ij} = \Delta_{ji}$ since the Hellinger distance is symmetric and $(\theta_{s_1}, \dots, \theta_{s_n})$ are exchangeable conditional on \mathbf{X} .
 - (c) $\Delta_{ih} \leq \Delta_{ij} + \Delta_{jh}$ since the triangle inequality in the Hellinger distance holds almost surely for $\theta_{s_i}, \theta_{s_j}, \theta_{s_h}$ conditional on \mathbf{X} .
3. Observe that

$$\begin{aligned} \Delta_{ij} &= \mathbb{E}_{\Pi}[\mathbb{E}_{\Pi}[h(g(\theta_{s_i}), g(\theta_{s_j})) \mid \lambda, \mathbf{X}] \mid \mathbf{X}] \\ &= \int_{\lambda} \sum_{m < l} \eta_{ml}^{(\lambda)} q_{ij}^{(\lambda)ml} d\Pi(\lambda \mid \mathbf{X}), \end{aligned}$$

where

$$\begin{aligned} q_{ij}^{(\lambda)ml} &= \Pi(\{s_i = l, s_j = m\} \cup \{s_i = m, s_j = l\} \mid \lambda, \mathbf{X}), \\ \eta_{ml}^{(\lambda)} &= h(g(\theta_m^{(\lambda)}), g(\theta_l^{(\lambda)})), \end{aligned}$$

for all $1 \leq m < l \leq L$. Since $\eta_{ml}^{(\lambda)} \leq 1$,

$$\Delta_{ij} \leq \int_{\lambda} \sum_{m < l} q_{ij}^{(\lambda)ml} d\Pi(\lambda \mid \mathbf{X}) = \Pi(s_i \neq s_j \mid \mathbf{X}).$$

\square

Appendix B Supplementary Material

B.1 Preliminaries for Asymptotic Results

Our proofs leverage on the mixing measure concentration results in [Nguyen \(2013\)](#); [Ho and Nguyen \(2016b\)](#), and [Guha et al. \(2021\)](#). We refer the reader to these papers for more information on many of the concepts and conditions we will discuss below. Our general strategy is as follows. First, we extrapolate convergence in the mixing measure to convergence of the weights and atoms. We then translate these convergence rates to the entries of Δ by exploiting the dependence of θ_{s_i} on λ .

B.1.1 Additional Notation

Given $x = (x_1, \dots, x_d)^T \in \mathbb{R}^d$, let $\|x\| = \sqrt{\sum_{s=1}^d x_s^2}$. We will only consider mixtures having identifiable mixing measures. That is, if $f^{(\lambda_1)}(x) = f^{(\lambda_2)}(x)$ for almost all x , then $\lambda_1 = \lambda_2$. This identifiability condition is satisfied by Gaussian mixtures, along with several exponential family mixtures ([Barndorff-Nielsen, 1965](#)) and location family mixtures ([Teicher, 1961](#)). Any parameters and quantities related to a mixture will be denoted in expanded notation to highlight the dependence on the mixing measure. For any $L \in \mathbb{N}$, let

$$\Lambda_L(\Theta) = \left\{ \lambda = \sum_{l=1}^L a_l^{(\lambda)} \delta_{\theta_l^{(\lambda)}} : \theta_l^{(\lambda)} \in \Theta, a_l^{(\lambda)} > 0 \forall l, \sum_{l=1}^L a_l^{(\lambda)} = 1 \right\},$$

and, for any $\lambda \in \Lambda_L(\Theta)$, let $f^{(\lambda)} = \sum_{l=1}^L a_l^{(\lambda)} g(\theta_l^{(\lambda)})$. We will also denote $\Omega_L(\Theta) = \bigcup_{l=1}^L \Lambda_l(\Theta)$, which is the set of mixing measures with at most L distinct components. For $p \geq 1$, the p -th order Wasserstein distance between the mixing measures $\lambda = \sum_{l=1}^L a_l^{(\lambda)} \delta_{\theta_l^{(\lambda)}}$ and $\tilde{\lambda} = \sum_{m=1}^{\tilde{L}} \tilde{a}_m^{(\tilde{\lambda})} \delta_{\tilde{\theta}_m^{(\tilde{\lambda})}}$ is

$$W_p(\lambda, \tilde{\lambda}) = \inf_{\mathbf{b} \in \mathcal{C}(\mathbf{a}^{(\lambda)}, \tilde{\mathbf{a}}^{(\tilde{\lambda})})} \left(\sum_{l,m} b_{lm} \left\| \theta_l^{(\lambda)} - \tilde{\theta}_m^{(\tilde{\lambda})} \right\|^p \right)^{1/p},$$

where $\mathcal{C}(\mathbf{a}^{(\lambda)}, \tilde{\mathbf{a}}^{(\tilde{\lambda})})$ is the set of all couplings with marginal distributions $\mathbf{a}^{(\lambda)}$ and $\tilde{\mathbf{a}}^{(\tilde{\lambda})}$. That is, for all $l = 1, \dots, L$, $\sum_{m=1}^{\tilde{L}} b_{lm} = a_l^{(\lambda)}$ and for all $m = 1, \dots, \tilde{L}$, $\sum_{l=1}^L b_{lm} = \tilde{a}_m^{(\tilde{\lambda})}$.

Recall that \mathbb{P}_0 refers to probability statements with respect to the true data generating process, with $\mathbb{P}_0(A) = \int_A f_0(x) dx$. Positive constants that do not depend on n will typically be denoted by M . For any sequences y_n and z_n , $y_n \lesssim z_n$ if there exists a $N \in \mathbb{N}$ and constant $B > 0$ so that $|y_n| \leq B|z_n|$ for all $n \geq N$; $y_n \asymp z_n$ if $y_n \lesssim z_n$ and $z_n \lesssim y_n$; and $y_n \sim z_n$ if $y_n/z_n \rightarrow 1$. A random variable $Z_n = o_{\mathbb{P}_0}(1)$ if $Z_n \rightarrow 0$ in \mathbb{P}_0 -probability.

B.2 Strong Identifiability and Lipschitz Conditions

As stated in [Section 3](#), Wasserstein contraction of λ will require that \mathcal{G} is strongly identifiable, referring to a linear independence condition on the derivatives of $g(x; \theta)$. We formally define

these concepts below. Recall that $\Theta \subset \mathbb{R}^d$ is assumed to be compact and $f^{(\lambda)}$ to be identifiable in λ . In these definitions, $\nabla_g(\theta)$ and $\mathbf{H}_g(\theta)$ denote the gradient and Hessian of $g(x; \theta)$ with respect to θ .

Definition B.1. The family $\mathcal{G} = \{g(\theta) : \theta \in \Theta\}$ is first order identifiable if $g(x; \theta)$ is differentiable in θ and, given r atoms $\theta_1, \dots, \theta_r \in \Theta$, if there exists $\beta_1, \dots, \beta_r \in \mathbb{R}$ and $\rho_1, \dots, \rho_r \in \mathbb{R}^d$ so that for all x

$$\sum_{s=1}^r \{\beta_s g(x; \theta_s) + \rho_s^T \nabla_g(\theta_s)\} = 0, \quad (33)$$

then $\beta_s = 0$ and $\rho_s = \mathbf{0}$ for all $s = 1, \dots, r$.

Definition B.2. The family $\mathcal{G} = \{g(\theta) : \theta \in \Theta\}$ is second order identifiable if $g(x; \theta)$ is twice differentiable in θ and, given r atoms $\theta_1, \dots, \theta_r \in \Theta$, if there exists $\beta_1, \dots, \beta_r \in \mathbb{R}$, $\rho_1, \dots, \rho_r \in \mathbb{R}^d$, and $\nu_1, \dots, \nu_r \in \mathbb{R}^d$ so that for all x

$$\sum_{s=1}^r \{\beta_s g(x; \theta_s) + \rho_s^T \nabla_g(\theta_s) + \nu_s^T \mathbf{H}_g(\theta_s) \nu_s\} = 0, \quad (34)$$

then $\beta_s = 0$ and $\rho_s = \nu_s = \mathbf{0}$ for all $s = 1, \dots, r$.

It is clear from the two definitions that second-order identifiability implies first-order identifiability. These notions are commonly used in the literature because they bridge the connection between convergence from f to f_0 (or f^*) in the Hellinger distance and convergence from λ to λ_0 (or λ^*) in Wasserstein distance. This will be useful for showing concentration of the weights and atoms, as this is straightforward to extract from convergence of the mixing measure. A canonical example of a second-order identifiable family are Gaussian location mixtures for a known covariance matrix Σ , i.e. $\mathcal{G} = \{\mathcal{N}_d(\theta, \Sigma) : \theta \in \Theta\}$.

Recall that we also impose Lipschitz conditions on the derivatives of $g(x; \theta)$. The strongest condition we make is the second order integral Lipschitz property, as introduced in [Guha et al. \(2021\)](#).

Definition B.3. \mathcal{G} satisfies the integral Lipschitz property of the second order with respect to the mixing measures λ_0 and λ_* if $g(x; \theta)$ is twice differentiable in θ and for all $x \in \chi$,

$$|\zeta^T (\mathbf{H}_g(\theta_1) - \mathbf{H}_g(\theta_2)) \zeta| \leq M(x) \|\theta_1 - \theta_2\|^\xi \|\zeta\|^2 \quad (35)$$

for any $\zeta \in \mathbb{R}^d$ and for some $\xi > 0$ that is independent of x and θ_1, θ_2 , where $M(x)$ is a function of x so that $\mathbb{E}_0[M(X)/f^*(X)] < \infty$.

Note that this is not only a condition on \mathcal{G} , but also on λ_0 and f_0 . The inequality in (35) is effectively a smoothness condition on the Hessian of $g(x; \theta)$, where the Lipschitz constant is a function of x . We will need to assume that the integral Lipschitz property holds in order to invoke concentration of the mixing measure for the misspecified regime, which is instrumental for proving Proposition 3. Related to the integral Lipschitz property is the uniform Lipschitz property, which was introduced in [Ho and Nguyen \(2016b\)](#).

Definition B.4. \mathcal{G} satisfies the uniform Lipschitz property of the second order if $g(x; \theta)$ is twice differentiable in θ and for all $x \in \mathcal{X}$,

$$|\zeta^T (\mathbf{H}_g(\theta_1) - \mathbf{H}_g(\theta_2)) \zeta| \leq M \|\theta_1 - \theta_2\|^\xi \|\zeta\|^2 \quad (36)$$

for any $\zeta \in \mathbb{R}^d$ and for some $\xi, M > 0$ that are independent of x and θ_1, θ_2 .

The uniform Lipschitz property will be useful when we consider the well-specified regime. As in (35), it is also a Lipschitz condition on the Hessian of $g(x; \theta)$. The second order Lipschitz property is satisfied by the location-scale Gaussian family and location-scale Student's t family (Ho et al., 2020).

Lipschitz conditions on the second derivatives of a probability density function are frequently assumed in the literature on mixing measure concentration. See, for example, Lemma 2 in Chen (1995) and Theorem 1 in Nguyen (2013). While it is difficult to characterize what choices of f_0 and \mathcal{G} can admit the integral Lipschitz property, the property will hold if \mathcal{G} is uniformly Lipschitz and $\int_{\mathbb{R}^2} \frac{f_0(x)}{f^*(x)} dx < \infty$. Hence, for uniformly Lipschitz families, such as location Gaussians, the integral Lipschitz property can be reformulated as a tail condition on f^* and f_0 .

B.3 Conditions and Wasserstein Concentration

For the overfitted and misspecified case, we require the following conditions.

Assumption 1. Suppose that the following conditions are satisfied by \mathcal{G} , Π , f_0 , and λ_0 .

(A1): The KL minimizer exists and is unique, with $K^* < L < \infty$.

(A2): The family \mathcal{G} is second-order identifiable and admits the uniform integral Lipschitz property up to the second order. Additionally, for any $x \in \mathbb{R}^d$, $g(x; \theta)$ is continuous in θ , and there exists a constant $M_0 > 0$ so that $\mathbb{P}_0(\max_{\theta \in \Theta} g(X; \theta) \leq M_0) = 1$. For any $\theta' \in \Theta$, $h(g(\theta), g(\theta'))$ is continuous at $\theta = \theta'$.

(A3): There exists an $\epsilon > 0$ so that $\mathbb{E}_0 \{f^*(X)/f^{(\lambda)}(X)\} \leq R^*(\epsilon)$ when $W_1(\lambda, \lambda_*) \leq \epsilon$ for any $\lambda \in \Omega_{K^*}(\Theta)$, where $R^*(\epsilon)$ is a function of ϵ that only depends on λ_* , λ_0 , and Θ .

(A4): $\Pi(\mathbf{a})$ is a symmetric Dirichlet prior, with concentration parameter $\alpha < 1$. $\Pi(\theta)$ is absolutely continuous with respect to the Lebesgue measure with probability density function $p(\theta)$, which satisfies $\int_{\Theta} p(\theta) d\theta = 1$ and $\min_{\theta \in \Theta} p(\theta) > 0$.

(A5): $\mathcal{G} = \{\tilde{g}(x - \theta) : \theta \in \Theta\}$ for some probability density function \tilde{g} . Also, there exists a $\zeta > 0$ so that $\tilde{g}(z)$ is ζ -Hölder continuous.

(A6): There exists a constant $\epsilon^* > 0$ so that $\mathbb{P}_0(f_*(X) \geq \epsilon^*) = 1$.

Condition (A2) is satisfied by location Gaussian mixtures when $\int_{\mathbb{R}^d} \frac{f_0(x)}{f^*(x)} dx < \infty$. Condition (A3) can be interpreted as a continuity condition on λ for convergence to f^* while averaging over f_0 . (A4) is a standard condition that is often implemented in Bayesian finite

mixtures. Similar to [Rousseau and Mengersen \(2011\)](#), we also have a threshold on α that determines the asymptotic behaviour of the weights. In contrast, our threshold is independent of dimension. (A6) essentially requires that f_* is a good approximation and that f_0 has bounded support, which will be useful for several of the bounds we show. In fact, (A6) is generally not needed, as $\mathbb{P}_0(f_*(X) \geq \epsilon_n) \rightarrow 1$ for any $\epsilon_n \rightarrow 0$ by the dominated convergence theorem. This would change [Theorem 1](#) to a high probability statement, rather than a probability equal to one statement, and lead to a slightly different form of the remainder in Δ_{ij}^{*+} (e.g. see [Theorem 4](#)). We next state a general result from [Guha et al. \(2021\)](#) on Wasserstein convergence of the mixing measure under these conditions.

Theorem 2. Let (A1)-(A4) hold. Then,

$$\Pi \left\{ \lambda \in \Lambda_L(\Theta) : W_2(\lambda, \lambda^*) \gtrsim (\log n/n)^{1/4} \mid \mathbf{X} \right\} \xrightarrow{\mathbb{P}_0} 0. \quad (37)$$

Proof. The proof is nearly identical to the proof of [Theorem 4.3](#) from [Guha et al. \(2021\)](#), in which the conditions of [Theorem C.2](#) from that article are verified. For sake of brevity and completeness, we do not redefine all the notation and concepts from their paper, but instead outline the modification of their proof to our case. We use the sieve $G_n = \Lambda_L(\Theta)$, and let ϵ_n denote a sequence such that $\epsilon_n \rightarrow 0$ and $\frac{n}{(\log(1/\epsilon_n))^2}$ is bounded away from 0. Conditions (A2) and (A3) allow us to lower bound the prior probability of a generalized Kullback-Leibler neighbourhood of λ^* with $\Pi(\lambda \in \Lambda_L(\theta) : W_1(\lambda, \lambda^*) \lesssim \epsilon_n^2)$. Under condition (A4), we invoke the proof of [Theorem 3.1](#) in [Guha et al. \(2021\)](#) and the tail bounds on the Dirichlet distribution given in [Lemma G.13](#) of [Ghosal and Van der Vaart \(2017\)](#) to show that

$$\Pi \left\{ \lambda \in \Lambda_L(\Theta) : W_1(\lambda, \lambda^*) \lesssim \epsilon_n^2 \right\} \gtrsim \epsilon_n^{2(c_\Pi + L\alpha)} \quad (38)$$

where $c_\Pi > 0$ depends on the prior $p(\theta)$. Finally, for the Hellinger information of G_n , $\bar{\Psi}_{G_n}(r) \geq \bar{\Psi}_{\Omega_L(\Theta)}(r) \gtrsim r^4$, implying that many of the derivations shown in the proof of [Theorem 4.3](#) of [Guha et al. \(2021\)](#) apply to our case as well. In particular, we can verify [Step 1](#) by setting $\epsilon_n = 1/n$ and $M_n = An^{3/4}(\log n)^{1/4}$, where $A > 0$ is a sufficiently large constant. [Step 2](#) naturally follows from our choice of sieves, as $\Pi(G_n) = 1$. Finally, using condition (A3) and the fact that $\bar{\Psi}_{G_n}(r) \gtrsim r^4$, [Step 3](#) is also verified by the proof of [Theorem 4.3](#) from [Guha et al. \(2021\)](#). \square

B.4 Proof of [Proposition 3](#)

Proof. We show concentration of the weights and atoms using a technique from [Nguyen \(2013\)](#). Let $\epsilon_n := (\log n/n)^{1/4}$, $0 < \delta < 1$, $a_{\min}^* = \min_h a_h^* > 0$, and fix $1 \leq h \leq K^*$.

$$\begin{aligned} M^2 \epsilon_n^2 &> W_2^2(\lambda, \lambda_*) \geq \sum_{l=1}^L b_{lh}^{(\lambda)} \left\| \theta_l^{(\lambda)} - \theta_h^* \right\|^2 \\ &\geq a_h^* \min_l \left\| \theta_l^{(\lambda)} - \theta_h^* \right\|^2 \geq a_{\min}^* \min_l \left\| \theta_l^{(\lambda)} - \theta_h^* \right\|^2. \end{aligned} \quad (39)$$

For large enough n , $a_{\min}^* \geq M^{2\delta} \epsilon_n^{2\delta}$, implying

$$W_2^{2(1-\delta)}(\lambda, \lambda_*) \geq \min_l \left\| \theta_l^{(\lambda)} - \theta_h^* \right\|^2. \quad (40)$$

Next, let

$$\mathcal{I}^{(\lambda)} = \left\{ l = 1, \dots, L : \exists h = 1, \dots, K^* \text{ such that } \min_l \left\| \theta_l^{(\lambda)} - \theta_h^* \right\|^2 \leq W_2^{2(1-\delta)}(\lambda, \lambda_*) \right\}, \quad (41)$$

and

$$\mathcal{I}_h^{(\lambda)} = \left\{ l = 1, \dots, L : \min_l \left\| \theta_l^{(\lambda)} - \theta_h^* \right\|^2 \leq W_2^{2(1-\delta)}(\lambda, \lambda_*) \right\}. \quad (42)$$

It follows that

$$W_2^2(\lambda, \lambda_*) \geq \sum_{l \notin \mathcal{I}^{(\lambda)}} a_l^{(\lambda)} \min_h \left\| \theta_l^{(\lambda)} - \theta_h^* \right\|^2 > W_2^{2(1-\delta)}(\lambda, \lambda_*) \sum_{l \notin \mathcal{I}^{(\lambda)}} a_l^{(\lambda)} \quad (43)$$

$$\implies \sum_{l \notin \mathcal{I}^{(\lambda)}} a_l^{(\lambda)} < W_2^{2\delta}(\lambda, \lambda_*) < M^{2\delta} \epsilon_n^{2\delta}. \quad (44)$$

Now, we will show concentration of the weights. For fixed h ,

$$\begin{aligned} M^2 \epsilon_n^2 > W_2(\lambda, \lambda_*) &\geq \sum_{l \in \mathcal{I}^{(\lambda)} \setminus \mathcal{I}_h^{(\lambda)}} b_{lh}^{(\lambda)} \left\| \theta_l^{(\lambda)} - \theta_h^* \right\|^2 \geq \min_{l \in \mathcal{I}^{(\lambda)} \setminus \mathcal{I}_h^{(\lambda)}} \left\| \theta_l^{(\lambda)} - \theta_h^* \right\|^2 \sum_{l \in \mathcal{I}^{(\lambda)} \setminus \mathcal{I}_h^{(\lambda)}} b_{lh}^{(\lambda)} \\ &= \min_{l \in \mathcal{I}^{(\lambda)} \setminus \mathcal{I}_h^{(\lambda)}} \left\| \theta_l^{(\lambda)} - \theta_h^* \right\|^2 \left(a_h^* - \sum_{l \in \mathcal{I}_h^{(\lambda)}} b_{lh}^{(\lambda)} - \sum_{l \notin \mathcal{I}^{(\lambda)}} b_{lh}^{(\lambda)} \right) \\ &= \min_{l \in \mathcal{I}^{(\lambda)} \setminus \mathcal{I}_h^{(\lambda)}} \left\| \theta_l^{(\lambda)} - \theta_h^* \right\|^2 \left(a_h^* - \sum_{l \in \mathcal{I}_h^{(\lambda)}} a_l^{(\lambda)} + \sum_{l \in \mathcal{I}_h^{(\lambda)}} \sum_{k \neq h} b_{lk}^{(\lambda)} - \sum_{l \notin \mathcal{I}^{(\lambda)}} b_{lh}^{(\lambda)} \right) \\ &\geq \min_{l \in \mathcal{I}^{(\lambda)} \setminus \mathcal{I}_h^{(\lambda)}} \left\| \theta_l^{(\lambda)} - \theta_h^* \right\|^2 \left(a_h^* - \sum_{l \in \mathcal{I}_h^{(\lambda)}} a_l^{(\lambda)} - \sum_{l \notin \mathcal{I}^{(\lambda)}} b_{lh}^{(\lambda)} \right) \\ &\geq \min_{l \in \mathcal{I}^{(\lambda)} \setminus \mathcal{I}_h^{(\lambda)}} \left\| \theta_l^{(\lambda)} - \theta_h^* \right\|^2 \left(a_h^* - \sum_{l \in \mathcal{I}_h^{(\lambda)}} a_l^{(\lambda)} - \sum_{l \in \mathcal{I}^{(\lambda)} \setminus \mathcal{I}_h^{(\lambda)}} b_{lh}^{(\lambda)} - \sum_{l \notin \mathcal{I}^{(\lambda)}} b_{lh}^{(\lambda)} \right) \\ &= \min_{l \in \mathcal{I}^{(\lambda)} \setminus \mathcal{I}_h^{(\lambda)}} \left\| \theta_l^{(\lambda)} - \theta_h^* \right\|^2 \left(\sum_{l \in \mathcal{I}_h^{(\lambda)}} b_{lh}^{(\lambda)} - \sum_{l \in \mathcal{I}_h^{(\lambda)}} a_l^{(\lambda)} \right) \\ &= - \min_{l \in \mathcal{I}^{(\lambda)} \setminus \mathcal{I}_h^{(\lambda)}} \left\| \theta_l^{(\lambda)} - \theta_h^* \right\|^2 \sum_{l \in \mathcal{I}_h^{(\lambda)}} \sum_{k \neq h} b_{lk}^{(\lambda)}. \end{aligned}$$

For any $k \neq h$, $m \in \mathcal{I}_k^{(\lambda)}$, and $l \in \mathcal{I}_h^{(\lambda)}$,

$$\begin{aligned} & \min_{l \in \mathcal{I}^{(\lambda)} \setminus \mathcal{I}_h^{(\lambda)}} \left\| \theta_l^{(\lambda)} - \theta_h^* \right\| \leq \left\| \theta_m^{(\lambda)} - \theta_h^* \right\| \\ & \leq \left\| \theta_m^{(\lambda)} - \theta_k^* \right\| + \left\| \theta_l^{(\lambda)} - \theta_k^* \right\| + \left\| \theta_l^{(\lambda)} - \theta_h^* \right\| \leq M\epsilon_n + \left\| \theta_l^{(\lambda)} - \theta_k^* \right\|. \end{aligned}$$

Since Θ is compact, this shows that

$$\begin{aligned} & - \min_{l \in \mathcal{I}^{(\lambda)} \setminus \mathcal{I}_h^{(\lambda)}} \left\| \theta_l^{(\lambda)} - \theta_h^* \right\|^2 \sum_{l \in \mathcal{I}_h^{(\lambda)}} \sum_{k \neq h} b_{lk}^{(\lambda)} \\ & \geq -M\epsilon_n - \sum_{l \in \mathcal{I}_h^{(\lambda)}} \sum_{k \neq h} b_{lk}^{(\lambda)} \left\| \theta_l^{(\lambda)} - \theta_k^* \right\|^2 \geq -M\epsilon_n - W_2(\lambda, \lambda_*)^2. \end{aligned}$$

Therefore, there is a positive constant $M > 0$ so that

$$\min_{l \in \mathcal{I}^{(\lambda)} \setminus \mathcal{I}_h^{(\lambda)}} \left\| \theta_l^{(\lambda)} - \theta_h^* \right\|^2 \left| a_h^* - \sum_{l \in \mathcal{I}_h^{(\lambda)}} a_l^{(\lambda)} - \sum_{l \notin \mathcal{I}_h^{(\lambda)}} b_{lh}^{(\lambda)} \right| \leq M\epsilon_n. \quad (45)$$

Observe that there exists $k \neq h$ and constant $M' > 0$ so that

$$\min_{l \in \mathcal{I}^{(\lambda)} \setminus \mathcal{I}_h^{(\lambda)}} \left\| \theta_l^{(\lambda)} - \theta_h^* \right\|^2 \geq \left\| \theta_h^* - \theta_k^* \right\|^2 - M\epsilon_n. \quad (46)$$

The above derivation implies that there exists constants M, M' , and $M'' > 0$ so that

$$\left| a_h^* - \sum_{l \in \mathcal{I}_h^{(\lambda)}} a_l^{(\lambda)} - \sum_{l \notin \mathcal{I}_h^{(\lambda)}} b_{lh}^{(\lambda)} \right| \leq \frac{M\epsilon_n}{\left\| \theta_h^* - \theta_k^* \right\|^2 - M'\epsilon_n} \quad (47)$$

$$\implies \left| a_h^* - \sum_{l \in \mathcal{I}_h^{(\lambda)}} a_l^{(\lambda)} \right| \leq \nu_n := \frac{M\epsilon_n}{\left\| \theta_h^* - \theta_k^* \right\|^2 - M'\epsilon_n} + (L - K^*)M''\epsilon_n^{2\delta} \lesssim \max(\epsilon_n, \epsilon_n^{2\delta}). \quad (48)$$

Finally, let

$$\mathcal{S}_n = \bigcap_{h=1}^{K^*} \bigcup_{\mathcal{I} \subset [L] \setminus \emptyset} \left\{ \max_{l \in \mathcal{I}} \left\| \theta_l - \theta_h^* \right\| \lesssim \epsilon_n, \left| \sum_{l \in \mathcal{I}} a_l - a_h^* \right| \lesssim \max(\epsilon_n, \epsilon_n^{2\delta}) \right\}, \quad (49)$$

$$\mathcal{T}_n = \bigcup_{\substack{\mathcal{I} \subset [L] \\ |\mathcal{I}| \leq R^*}} \left\{ \sum_{l \in \mathcal{I}} a_l \lesssim \epsilon_n^{2\delta} \right\}. \quad (50)$$

We have shown that for all $n \geq N$, $\Pi(\mathcal{S}_n \cap \mathcal{T}_n \mid \mathbf{X}) \geq \Pi(W_2(\lambda, \lambda^*) < M\epsilon_n \mid \mathbf{X})$, and so, by Theorem 2, $\Pi(\mathcal{S}_n \cap \mathcal{T}_n \mid \mathbf{X}) \xrightarrow{\mathbb{P}_0} 1$. Proposition 3 follows by applying the dominated convergence theorem. \square

B.5 Proof of Theorem 1

Proof. Let $\epsilon_n = (\log n/n)^{1/4}$. Under (A1)-(A4), Theorem 2 implies that for large enough n ,

$$\Delta_{ij} = \int_{B_{W_2}^{(n)}(\lambda_*)} \sum_{m < l} \eta_{ml}^{(\lambda)} q_{ij}^{ml(\lambda)} d\Pi(\lambda | \mathbf{X}) + o_{\mathbb{P}_0}(1), \quad (51)$$

where $B_{W_2}^{(n)} = \{\lambda \in \Lambda_L(\Theta) : W_2(\lambda, \lambda_*) < M\epsilon_n\}$ for some constant $M > 0$. Observe that we can decompose the integrand in (51):

$$\sum_{m < l} \eta_{ml}^{(\lambda)} q_{ij}^{ml(\lambda)} \quad (52)$$

$$= \sum_{l, m \in \mathcal{I}^{(\lambda)}} \eta_{ml}^{(\lambda)} q_{ij}^{ml(\lambda)} + \sum_{(l \notin \mathcal{I}^{(\lambda)}) \text{ or } (m \notin \mathcal{I}^{(\lambda)})} \eta_{ml}^{(\lambda)} q_{ij}^{ml(\lambda)} \quad (53)$$

$$= \sum_{h=1}^{K^*} \sum_{l, m \in \mathcal{I}_h^{(\lambda)}} \eta_{ml}^{(\lambda)} q_{ij}^{ml(\lambda)} + \sum_{h < k} \sum_{\substack{l \in \mathcal{I}_h^{(\lambda)} \\ m \in \mathcal{I}_k^{(\lambda)}}} \eta_{ml}^{(\lambda)} q_{ij}^{ml(\lambda)} + \sum_{(l \notin \mathcal{I}^{(\lambda)}) \text{ or } (m \notin \mathcal{I}^{(\lambda)})} \eta_{ml}^{(\lambda)} q_{ij}^{ml(\lambda)}. \quad (54)$$

For brevity, let $H(\theta, \theta') := h(g(\theta), g(\theta'))$ and $\psi_h^*(\theta) = H(\theta, \theta_h^*)$. By (A2), Lemma 1, and Remark 1, for any $1 \leq h \leq K^*$,

$$\max_{l \in \mathcal{I}_h^{(\lambda)}} H(\theta_l^{(\lambda)}, \theta_h^*) \leq \kappa_{nh} = \max_{\theta: \|\theta - \theta_h^*\| \leq M\epsilon_n} \varphi_h^*(\theta) \quad (55)$$

and $\kappa_{nh} \rightarrow 0$. Let $\kappa_n := \max_{h=1, \dots, K^*} \kappa_{nh}$. Then, for any $l, m \in \mathcal{I}_h^{(\lambda)}$,

$$H(\theta_l^{(\lambda)}, \theta_m^{(\lambda)}) \leq 2\kappa_n. \quad (56)$$

and for any $l \in \mathcal{I}_h^{(\lambda)}, m \in \mathcal{I}_k^{(\lambda)}$,

$$H(\theta_h^*, \theta_k^*) - 2\kappa_n \leq H(\theta_l^{(\lambda)}, \theta_m^{(\lambda)}) \leq H(\theta_h^*, \theta_k^*) + 2\kappa_n. \quad (57)$$

(A5) implies similar concentration for the densities at X_i and X_j . For $X \sim f_0$,

$$\begin{aligned} |g(X; \theta_l^{(\lambda)}) - g(X; \theta_h^*)| &= |\tilde{g}(X - \theta_l^{(\lambda)}) - \tilde{g}(X - \theta_h^*)| \\ &\leq M \left\| X - \theta_l^{(\lambda)} - \theta_h^* - X \right\|^\zeta = M \left\| \theta_l^{(\lambda)} - \theta_h^* \right\|^\zeta \leq M\epsilon_n^\zeta. \end{aligned}$$

Let $\xi_n = M\epsilon_n^\zeta$. It follows that,

$$\left| \sum_{h=1}^{K^*} \sum_{l \in \mathcal{I}_h^{(\lambda)}} a_l^{(\lambda)} g(X_i; \theta_l^{(\lambda)}) - f^*(X_i) \right| \lesssim \max(\xi_n, \nu_n) \quad (58)$$

where ν_n is defined in (48). Condition (A6) implies that for large n , the following holds with \mathbb{P}_0 -probability 1,

$$0 \leq f_-^{(n)}(X_i) \leq f^{(\lambda)}(X_i) \leq f_+^{(n)}(X_i) + M\epsilon_n^{2\delta}, \quad (59)$$

where

$$f_-^{(n)}(X_i) = f^*(X_i) - M \max(\xi_n, \nu_n); \quad (60)$$

$$f_+^{(n)}(X_i) = f^*(X_i) + M \max(\xi_n, \nu_n). \quad (61)$$

We can now begin to bound some of the terms in (54). For any $m, l \notin \mathcal{I}^{(\lambda)}$,

$$0 \leq q_{ij}^{ml(\lambda)} \quad (62)$$

$$= a_l^{(\lambda)} a_m^{(\lambda)} \frac{g(X_i; \theta_l^{(\lambda)})g(X_j; \theta_m^{(\lambda)}) + g(X_i; \theta_m^{(\lambda)})g(X_j; \theta_l^{(\lambda)})}{f^{(\lambda)}(X_i)f^{(\lambda)}(X_j)} \quad (63)$$

$$\leq \frac{M\epsilon_n^{4\delta}}{f_-^{(n)}(X_i)f_-^{(n)}(X_j)}. \quad (64)$$

Similarly, for any $l \notin \mathcal{I}^{(\lambda)}$ and $m \in \mathcal{I}^{(\lambda)}$,

$$0 \leq q_{ij}^{ml(\lambda)} \leq \frac{M\epsilon_n^{2\delta}}{f_-^{(n)}(X_i)f_-^{(n)}(X_j)}. \quad (65)$$

Next, if $l, m \in \mathcal{I}_h^{(\lambda)}$, by (56),

$$0 \leq \eta_{ml}^{(\lambda)} q_{ij}^{ml(\lambda)} \leq 2\kappa_n. \quad (66)$$

For any h, k ,

$$\left| \sum_{\substack{l \in \mathcal{I}_h^{(\lambda)} \\ m \in \mathcal{I}_k^{(\lambda)}}} a_l^{(\lambda)} a_m^{(\lambda)} g(X_i; \theta_l^{(\lambda)})g(X_j; \theta_m^{(\lambda)}) - a_h^* a_k^* g(X_i; \theta_h^*)g(X_j; \theta_k^*) \right| \lesssim \max(\xi_n, \nu_n) \quad (67)$$

Therefore,

$$(\eta_{hk}^* - 2\kappa_n)R_{ij}^{hk} \leq \sum_{\substack{l \in \mathcal{I}_h^{(\lambda)} \\ m \in \mathcal{I}_k^{(\lambda)}}} \eta_{ml}^{(\lambda)} q_{ij}^{ml(\lambda)} \leq (\eta_{hk}^* + 2\kappa_n)S_{ij}^{hk}; \quad (68)$$

$$R_{ij}^{hk} = \frac{a_h^* a_k^* \{g(X_i; \theta_h^*)g(X_j; \theta_k^*) + g(X_j; \theta_h^*)g(X_i; \theta_k^*)\} - M \max(\xi_n, \nu_n)}{(f_+^{(n)}(X_i) + M\epsilon_n^{2\delta})(f_+^{(n)}(X_j) + M\epsilon_n^{2\delta})}; \quad (69)$$

$$S_{ij}^{hk} = \frac{a_h^* a_k^* \{g(X_i; \theta_h^*)g(X_j; \theta_k^*) + g(X_j; \theta_h^*)g(X_i; \theta_k^*)\} + M \max(\xi_n, \nu_n)}{f_-^{(n)}(X_i)f_-^{(n)}(X_j)}. \quad (70)$$

Finally, this gives us the following bound on (54) for all $\lambda \in B_{W_2}^{(n)}(\lambda_*)$,

$$\Delta_{ij}^{*-} \leq \sum_{m < l} \eta_{ml}^{(\lambda)} q_{ij}^{ml(\lambda)} \leq \Delta_{ij}^{*+}, \quad (71)$$

$$(72)$$

where

$$\Delta_{ij}^{*-} := \sum_{h < k} (\eta_{hk^*} - 2\kappa_n) R_{ij}^{hk}; \quad (73)$$

$$\Delta_{ij}^{*+} := K^*(R^* + 1)R^*\kappa_n + \sum_{h < k} (\eta_{hk}^* + 2\kappa_n) S_{ij}^{hk} + \frac{M \left\{ \binom{L}{2} - \binom{K^*}{2} \right\} \epsilon_n^{2\delta}}{f_-^{(n)}(X_i) f_-^{(n)}(X_j)}. \quad (74)$$

□

Lemma 1. Let $\chi \subset \mathbb{R}^d$ be compact and $f : \chi \rightarrow \mathbb{R}$, where f is bounded on χ and f is continuous at a point $y \in \chi$. Let δ_n be a sequence with $\lim_{n \rightarrow \infty} \delta_n = 0$ and $B_{\delta_n}(y) = \{x \in \chi : \|x - y\| \leq \delta_n\}$. Then, there exists a sequence ϵ_n that only depends only y and with $\lim_{n \rightarrow \infty} \epsilon_n = 0$ so that for all $x \in B_{\delta_n}(y)$,

$$|f(x) - f(y)| \leq \epsilon_n. \quad (75)$$

Proof. Consider sequences of within-neighbourhood maximizers and minimizers of f ,

$$x_n = \operatorname{argmax}_{x \in B_{\delta_n}(y)} f(x); \quad (76)$$

$$z_n = \operatorname{argmin}_{x \in B_{\delta_n}(y)} f(x). \quad (77)$$

In the case where there are multiple minimizers or maximizers, simply choose one of these points as x_n or z_n . Since f is continuous and bounded and $B_{\delta_n}(y)$ is a compact set, $x_n, z_n \in B_{\delta_n}(y)$. This means that $x_n \rightarrow y$ and $z_n \rightarrow y$, which implies $f(x_n) \rightarrow f(y)$ and $f(z_n) \rightarrow f(y)$ by continuity. Therefore, for any $x \in B_{\delta_n}(y)$,

$$|f(x) - f(y)| \leq \epsilon_n := |f(x_n) - f(z_n)| \rightarrow 0. \quad (78)$$

□

Remark 1. Observe that if $y = \operatorname{argmin}_{x \in \chi} f(x)$, the proof of Lemma 1 implies that we can instead set $\epsilon_n = |f(x_n) - f(y)|$.

B.6 The Well-Specified Case

When the model is well-specified, we assume that $f_0 = \sum_{h=1}^{K_0} a_h^0 g(\theta_h^0)$ for some $\theta_1^0, \dots, \theta_{K_0}^0 \in \Theta$ and $a_h^0 > 0$, $\sum_{h=1}^{K_0} a_h^0 = 1$. In turn, the posterior distribution of λ will contract towards $\lambda_0 = \sum_{h=1}^{K_0} a_h^0 \delta_{\theta_h^0}$. For finite mixtures, the disparity $R_0 = L - K_0$ between the number of components in the true state of nature f_0 and the number of components in f will affect the contraction rate. Under an *exact-fitted* mixture, where $K_0 = L$, the contraction rate is given by $(\log n/n)^{1/2}$ (Nguyen, 2013; Ho and Nguyen, 2016a). When $K_0 < L$, the model is overfitted, and λ contracts to λ_0 at the slower rate of $(\log n/n)^{1/4}$ (Nguyen, 2013; Ho and Nguyen, 2016a; Guha et al., 2021). Observe that this rate is identical to the contraction rate of λ to λ^* in the misspecified case.

Our conditions for the well-specified case are similar to the misspecified case. In particular, we will still need second-order identifiability and a Lipschitz condition.

Assumption 2. We impose the following conditions on \mathcal{G} , Π , f_0 , and λ_0 .

(C1): f_0 is a finite mixture, with $K_0 < L < \infty$.

(C2): The family \mathcal{G} is second-order identifiable and admits the uniform Lipschitz property up to the second order. Additionally, for any $x \in \mathbb{R}^d$, $g(x; \theta)$ is continuous in θ , and there exists a constant $M_0 > 0$ so that $\mathbb{P}_0(\max_{\theta \in \Theta} g(X; \theta) \leq M_0) = 1$. For any $\theta' \in \Theta$, $h(g(\theta), g(\theta'))$ is continuous at $\theta = \theta'$.

(C3): $\Pi(\mathbf{a})$ and $\Pi(\theta)$ satisfy condition (A4) in Assumption 1.

(C4): \mathcal{G} satisfies condition (A5) in Assumption 1.

As in the misspecified case, the canonical example for which conditions (C1)-(C4) apply is a mixture of location Gaussian kernels. We can now state the formal result on posterior contraction of the mixing measure for the well-specified case.

Theorem 3. Let (C1)-(C4) hold. Then,

$$\Pi \left\{ \lambda \in \Lambda_L(\Theta) : W_2(\lambda, \lambda_0) \gtrsim (\log n/n)^{1/4} \right\} \xrightarrow{\mathbb{P}_0} 0. \quad (79)$$

Proof. See [Nguyen \(2013\)](#) and [Guha et al. \(2021\)](#). \square

We then reformulate Theorem 3 in terms of the atoms and weights so that we can show concentration of Δ .

Proposition 4. Let $\epsilon_n = (\log n/n)^{1/4}$ and $0 < \delta < 1$. For any $h \in [K_0]$ and $\mathcal{I} \in [L]$, define the events

$$A_{h,\mathcal{I}} = \left\{ \max_{l \in \mathcal{I}} \|\theta_l - \theta_h^0\| \lesssim \epsilon_n, \left| \sum_{l \in \mathcal{I}} a_l - a_h^0 \right| \lesssim (\epsilon_n \vee \epsilon_n^{2\delta}) \right\}, \quad B_{\mathcal{I}} = \left\{ \sum_{l \in \mathcal{I}} a_l \lesssim \epsilon_n^{2\delta} \right\}. \quad (80)$$

Then under conditions (C1)-(C4), as $n \rightarrow \infty$,

$$\mathbb{E}_0 \left[\Pi \left\{ \left(\bigcap_{h=1}^{K_0} \bigcup_{|\mathcal{I}| \geq 1} A_{h,\mathcal{I}} \right) \cap \left(\bigcup_{|\mathcal{I}| \leq R_0} B_{\mathcal{I}} \right) \mid \mathbf{X} \right\} \right] \rightarrow 1. \quad (81)$$

Proof. The result can be shown using the same technique as the proof for Proposition 3, but a_h^* and θ_h^* are exchanged with a_h^0 and θ_h^0 . \square

In contrast to the misspecified regime, \mathbf{c}_{FOLD} will contract towards the oracle FOLD clusters. We define these as

$$\mathbf{c}_{\text{FOLD}}^{\text{oracle}} = \underset{\hat{\mathbf{c}}}{\operatorname{argmin}} \sum_{i < j} \{ \mathbf{1}_{\hat{c}_i = \hat{c}_j} \Delta_{ij}^0 + \omega \mathbf{1}_{\hat{c}_i \neq \hat{c}_j} (1 - \Delta_{ij}^0) \}, \quad (82)$$

where $\Delta_{ij}^0 = \mathbb{E}_{\Pi}[\mathcal{H}_{ij} \mid \mathbf{X}, \lambda_0]$. That is, the oracle FOLD clusters arise when the true data generating process is known. We can then rewrite Δ_{ij}^0 as

$$\Delta_{ij}^0 = \sum_{h < k} h \{ g(\theta_h^0), g(\theta_k^0) \} \frac{a_h^0 a_k^0 \{ g(X_i; \theta_h^0) g(X_j; \theta_k^0) + g(X_i; \theta_k^0) g(X_j; \theta_h^0) \}}{f_0(X_i) f_0(X_j)}. \quad (83)$$

Δ_{ij}^0 are a weighted sum of the pairwise Hellinger distances between the component kernels in f_0 . We can now state our main result on contraction to the oracle clusters.

Theorem 4. Let $\epsilon_n = (\log n/n)^{1/4}$, $0 < \delta < 1$, and assume conditions (C1)-(C4) hold. Then, for all $n \geq N$ for some $N \in \mathbb{N}$ and fixed $i < j$, there exists a constant $M > 0$ and random variables $\Delta_{ij}^{0-} = \Delta_{ij}^0 - o_{\mathbb{P}_0}(1)$ and

$$\Delta_{ij}^{0+} = \Delta_{ij}^0 + o_{\mathbb{P}_0}(1) + \frac{M \left\{ \binom{L}{2} - \binom{K_0}{2} \right\} \epsilon_n^{2\delta}}{f_0(X_i)f_0(X_j) - o_{\mathbb{P}_0}(1)} + \frac{o_{\mathbb{P}_0}(1)}{f_0(X_i)f_0(X_j) - o_{\mathbb{P}_0}(1)} \quad (84)$$

so that with \mathbb{P}_0 -probability tending to 1,

$$\Delta_{ij}^{0-}(1 - o_{\mathbb{P}_0}(1)) + o_{\mathbb{P}_0}(1) \leq \Delta_{ij} \leq \Delta_{ij}^{0+}(1 - o_{\mathbb{P}_0}(1)) + o_{\mathbb{P}_0}(1). \quad (85)$$

Remark 2. Note that we state (85) as a high probability statement, not an almost everywhere statement. Pragmatically, this is because of (59), as we will need to show

$$f_0(X) \geq M \max(\epsilon_n, \nu_n) \quad (86)$$

in order for us to construct Δ_{ij}^{0-} and Δ_{ij}^{0+} without dealing with negative numbers that could change the direction of the inequalities. It is simple to verify that the probability of (86) goes to 1 for any probability density function f_0 by the dominated convergence theorem.

Proof. The proof is nearly identical to that of Theorem 1, with two exceptions. First, (59) is not satisfied with \mathbb{P}_0 -probability equal to one, but rather \mathbb{P}_0 -probability tending to 1. More formally, $\mathbb{P}_0(\Delta_{ij} \leq \Delta_{ij}^{0+}) \rightarrow 1$, so the \mathbb{P}_0 -probability of (85) goes to 1 as $n \rightarrow \infty$ as well. Second, we must be a little more careful in this case when expanding the middle term in (74), as we cannot necessarily assume that there is some positive ϵ with $\mathbb{P}_0(f_0(X_i) \geq \epsilon) = 1$. Hence, we have an extra remainder term in Δ_{ij}^{0+} , though as before, we expect this remainder term to be arbitrarily small in the large sample limit. \square

Remark 3. A special case is the location mixture of Gaussians. Here, we have that

$$\mathbb{P}_0 \left\{ \mathcal{N}_d(X; \theta_h^0; \Sigma) \geq M \max(\epsilon_n, \nu_n) \mid s_0 = h \right\} \quad (87)$$

$$= \mathbb{P}_0 \left[\left\| \Sigma^{-1/2}(X - \theta_h^0) \right\|^2 \leq -2 \log \left\{ (2\pi)^{d/2} \det(\Sigma)^{1/2} M \max(\epsilon_n, \nu_n) \right\} \mid s_0 = h \right] \quad (88)$$

$$\geq 1 + \frac{d}{2 \log \left\{ (2\pi)^{d/2} \det(\Sigma)^{1/2} M \max(\epsilon_n, \nu_n) \right\}} \quad (89)$$

by Markov's inequality as $\left\| \Sigma^{-1/2}(X - \theta_h^0) \right\|^2 \sim \chi_d^2$. If we set $a_{\min}^0 = \min_h a_h^0$, we then have that for any $M > 0$,

$$\mathbb{P}_0 \left\{ f_0(X) \geq M \max(\epsilon_n, \nu_n) \right\} = \sum_{h=1}^{K_0} a_h^0 \mathbb{P}_0 \left\{ f_0(X) \geq M \max(\epsilon_n, \nu_n) \mid s_0 = h \right\} \quad (90)$$

$$\geq \sum_{h=1}^{K_0} a_h^0 \mathbb{P}_0 \left\{ \mathcal{N}_d(X; \theta_h^0; \Sigma) \geq \frac{M}{a_h^0} \max(\epsilon_n, \nu_n) \mid s_0 = h \right\} \quad (91)$$

$$\geq \sum_{h=1}^{K_0} a_h^0 \mathbb{P}_0 \left\{ \mathcal{N}_d(X; \theta_h^0; \Sigma) \geq \frac{M}{a_{\min}^0} \max(\epsilon_n, \nu_n) \mid s_0 = h \right\} \quad (92)$$

$$= \mathbb{P}_0 \left\{ \mathcal{N}_d(X; \theta_h^0; \Sigma) \geq \frac{M}{a_{\min}^0} \max(\epsilon_n, \nu_n) \mid s_0 = h \right\}, \quad (93)$$

because (89) does not depend on h . This tells us that the \mathbb{P}_0 probability of (86) goes to 1 at an approximately $\log(\log n/n)$ rate.

B.7 Additional Details on Credible Balls

We express uncertainty in \mathbf{c}_{FOLD} using a 95% credible ball. For visualizations, we rely on the notions of horizontal and vertical bounds, as introduced in [Wade and Ghahramani \(2018\)](#). For completeness, we include the formal definitions of these bounds below. The horizontal bounds are given by the clusterings in $B_D(\mathbf{c}_{\text{FOLD}})$ furthest from \mathbf{c}_{FOLD} by $D(\cdot, \cdot)$.

Definition B.5. The horizontal bound(s) of $B_D(\mathbf{c}_{\text{FOLD}})$ are

$$H(\mathbf{c}_{\text{FOLD}}) = \{\mathbf{c} \in B_D(\mathbf{c}_{\text{FOLD}}) : D(\mathbf{c}, \mathbf{c}_{\text{FOLD}}) \geq D(\mathbf{c}', \mathbf{c}_{\text{FOLD}}) \forall \mathbf{c}' \in B_D(\mathbf{c}_{\text{FOLD}})\}.$$

For any clustering \mathbf{c} , let $K_{\mathbf{c}}$ be the number of clusters. The vertical bounds also consider clusterings in $B_D(\mathbf{c}_{\text{FOLD}})$ that are far from \mathbf{c}_{FOLD} , but impose additional constraints on the number of clusters.

Definition B.6. The vertical upper bound(s) of $B_D(\mathbf{c}_{\text{FOLD}})$ are

$$\begin{aligned} \text{VU}(\mathbf{c}_{\text{FOLD}}) &= \{\mathbf{c} \in B_D(\mathbf{c}_{\text{FOLD}}) : K_{\mathbf{c}} \leq K_{\mathbf{c}'} \forall \mathbf{c}' \in B_D(\mathbf{c}_{\text{FOLD}}), \\ &D(\mathbf{c}, \mathbf{c}_{\text{FOLD}}) \geq D(\mathbf{c}', \mathbf{c}_{\text{FOLD}}) \forall \mathbf{c}' \in B_D(\mathbf{c}_{\text{FOLD}}) \text{ with } K_{\mathbf{c}} = K_{\mathbf{c}'}\}. \end{aligned}$$

Definition B.7. The vertical lower bound(s) of $B_D(\mathbf{c}_{\text{FOLD}})$ are

$$\begin{aligned} \text{VL}(\mathbf{c}_{\text{FOLD}}) &= \{\mathbf{c} \in B_D(\mathbf{c}_{\text{FOLD}}) : K_{\mathbf{c}} \geq K_{\mathbf{c}'} \forall \mathbf{c}' \in B_D(\mathbf{c}_{\text{FOLD}}), \\ &D(\mathbf{c}, \mathbf{c}_{\text{FOLD}}) \geq D(\mathbf{c}', \mathbf{c}_{\text{FOLD}}) \forall \mathbf{c}' \in B_D(\mathbf{c}_{\text{FOLD}}) \text{ with } K_{\mathbf{c}} = K_{\mathbf{c}'}\}. \end{aligned}$$

In practice, we compute the credible balls using the R function `credibleball()` ([Wade, 2015](#)). $D(\cdot, \cdot)$ can be either the Variation of Information distance or Binder’s loss.

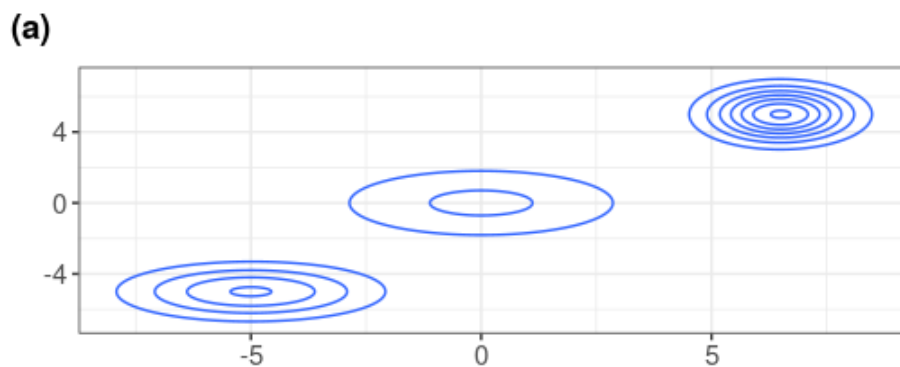
B.8 Additional Details on Simulations

The goal of our simulations is to show that FOLD can perform reliably when n increases, counteracting the fact that larger sample size will result in more and more non-empty components in our mixture. We set $L = 30$, the Normal-Inverse-Wishart prior parameters to be $\mu = 0_d$, $\kappa = 1$, $\nu = d + 2$, and $\Psi = \mathbf{I}_d$, and the Dirichlet concentration parameter for \mathbf{a} is $\alpha = 1/2$. The rationale behind setting $\alpha = 1/2$ is to keep the number of non-empty components in f large, ensuring that we are approximating f_0 with f , while also trying to recreate the settings of our theoretical results. We additionally hope to validate ω^{AVG} as a reasonable loss parameter for Gaussian mixtures.

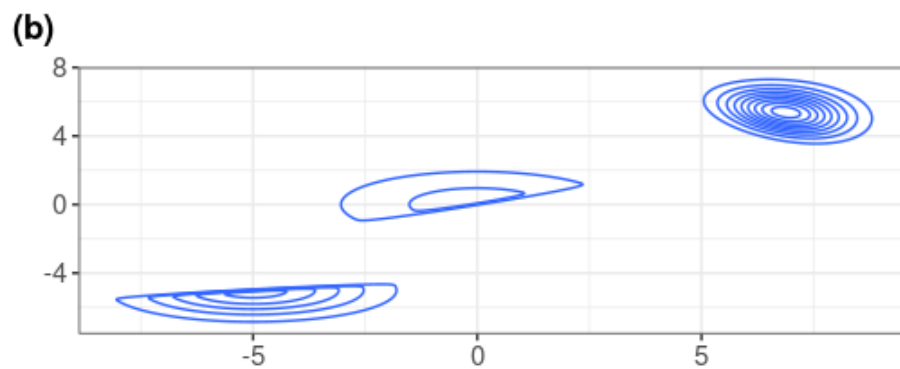
B.8.1 Mixture of Bivariate Gaussian Kernels

We sample from a distribution of $K_0 = 3$ multivariate skew normal kernels;

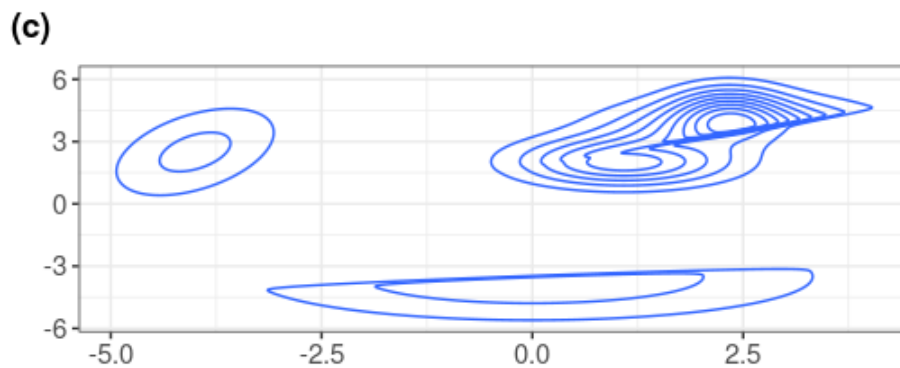
$$f_0(x) = 0.45 \tau_{01}(x) + 0.25 \tau_{02}(x) + 0.3 \tau_{03}(x); \tag{94}$$



Contours of the Gaussian mixture.



Contours of the Skew Gaussian mixture.



Contours of the Skew-Symmetric mixture.

Figure 11: Contour plots of the (a) Gaussian mixture, (b) skew Gaussian mixture and (c) skew-symmetric mixture.

where

$$\tau_{01} = \mathcal{N}_d \left(\begin{pmatrix} 6.5 \\ 5 \end{pmatrix}, \mathbf{I}_d \right), \quad (95)$$

$$\tau_{02} = \mathcal{SN}_d \left(\begin{pmatrix} 0 \\ 0 \end{pmatrix}, \text{diag}(5, 2) \right); \quad (96)$$

$$\tau_{03} = \mathcal{SN}_d \left(\begin{pmatrix} -5 \\ -5 \end{pmatrix}, \text{diag}(3, 1) \right). \quad (97)$$

using the `mvtnorm` package (Genz and Bretz, 2009; Genz et al., 2021). A contour plot of f_0 is given in Figure 11(a). The kernel parameters are chosen so that the components of f_0 are well separated in \mathbb{R}^2 . Given a sample size n , we sample $X_1, \dots, X_n \sim f_0$, then fit a location-scale Gaussian mixture to the data. The fundamental idea behind this example is to show that FOLD performs well in the best of scenarios: when the model is well-specified and the kernels of f_0 do not overlap. Unlike the other examples we consider, we have access to the oracle FOLD clusters (82), which are computed every replication along with `cFOLD`, the VI clusters, Binder’s clusters, and the `mclust` clusters.

B.8.2 Mixture of Bivariate Skew Gaussian Kernels

We sample from a distribution of $K_0 = 3$ multivariate skew normal kernels;

$$f_0(x) = 0.45 \cdot \tau_{01}(x) + 0.25 \cdot \tau_{02}(x) + 0.3 \cdot \tau_{03}(x); \quad (98)$$

where

$$\tau_{01} = \mathcal{SN}_d \left(\begin{pmatrix} 6.5 \\ 5 \end{pmatrix}, \mathbf{I}_d, \begin{pmatrix} 1 \\ 1 \end{pmatrix} \right); \quad (99)$$

$$\tau_{02} = \mathcal{SN}_d \left(\begin{pmatrix} 0 \\ 0 \end{pmatrix}, \text{diag}(5, 2), \begin{pmatrix} -10 \\ 15 \end{pmatrix} \right); \quad (100)$$

$$\tau_{03} = \mathcal{SN}_d \left(\begin{pmatrix} -5 \\ -5 \end{pmatrix}, \text{diag}(3, 1), \begin{pmatrix} 4 \\ -17 \end{pmatrix} \right); \quad (101)$$

using the `sn` package (Azzalini, 2022). A contour plot of f_0 in this case is given in Figure 11(b). The kernel parameters are chosen so that τ_{01} , τ_{02} , and τ_{03} are well-separated in \mathbb{R}^2 , but diverge from Gaussianity. As before, we sample $X_1, \dots, X_n \sim f_0$, then centre and scale \mathbf{X} and fit a Gaussian mixture. The motivation behind using skew Gaussian kernels is to show how even a relatively small amount of model misspecification can lead to poor clustering results, especially with `mclust` and Binder’s loss. We find that both FOLD and VI are more robust to this perturbation from Gaussianity, consistently computing a small number of clusters with high adjusted Rand index with \mathbf{s}_0 .

B.8.3 Skew-Symmetric Mixture

Finally, we sample from a mixture of $K_0 = 3$ kernels. We formulate f_0 as

$$f_0(x) = 0.55 \cdot \tau_{01}(x) + 0.3 \cdot \tau_{02}(x) + 0.15 \cdot \tau_{03}(x); \quad (102)$$

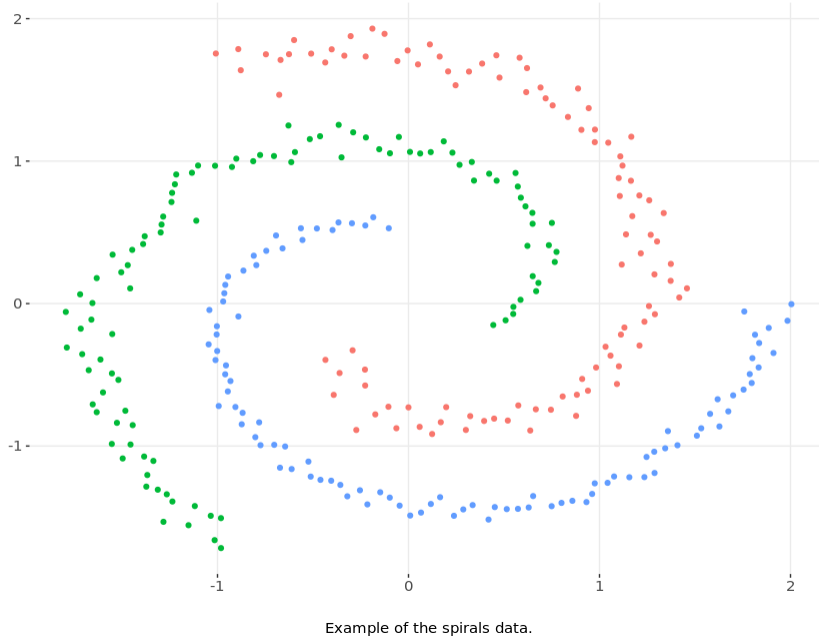


Figure 12: A sample of $n = 300$ observations with the `spirals()` function, with colours corresponding to \mathbf{s}_0 . The thin, interlocking nature of the spirals make this dataset a difficult problem for clustering algorithms.

where

$$\tau_{01} = 0.364 \cdot \mathcal{SN}_d \left(\begin{pmatrix} 2.50 \\ 3.50 \end{pmatrix}, \mathbf{I}_d, \begin{pmatrix} -10 \\ 15 \end{pmatrix} \right) + \quad (103)$$

$$0.212 \cdot \mathcal{N}_d \left(\begin{pmatrix} 2.325 \\ 4.381 \end{pmatrix}, \text{diag}(0.20, 0.80) \right) + \quad (104)$$

$$0.424 \cdot \mathcal{N}_d \left(\begin{pmatrix} 1.085 \\ 2.009 \end{pmatrix}, \text{diag}(0.70, 0.60) \right); \quad (105)$$

$$\tau_{02} = \mathcal{SN}_d \left(\begin{pmatrix} 0 \\ -3.50 \end{pmatrix}, \text{diag}(5, 2), \begin{pmatrix} 4 \\ -17 \end{pmatrix} \right); \quad (106)$$

$$\tau_{03} = \mathcal{N}_d \left(\begin{pmatrix} -4 \\ -2.50 \end{pmatrix}, \begin{pmatrix} 0.50 & 0.50 \\ 0.50 & 2.50 \end{pmatrix} \right). \quad (107)$$

The kernel parameters are chosen so that the data can be allocated into 3 clusters, with one of the clusters being a mixture of one skew Gaussian kernel and two Gaussian kernels. See Figure 11(c) for a contour plot of f_0 . Our intention with this example is to show that FOLD will tend to select 3-4 clusters despite one cluster itself being a mixture. As with the previous examples, we sample $X_1, \dots, X_n \sim f_0$, then centre and scale the data.

B.8.4 Validation of Credible Balls

In this section, we focus on the 95% credible ball around \mathbf{c}_{FOLD} . We simulate from a notably difficult scenario for clustering, the `spirals` dataset, as generated from the `KODAMA` package

Avg. $\text{VI}(\mathbf{s}_0, \mathbf{c}_{\text{FOLD}}) \leq \text{VI}(\mathbf{c}_H, \mathbf{c}_{\text{FOLD}})$	Avg. No. of Clusters (SD)	Avg. ARI (SD)
0.890	3.120 (0.327)	0.223 (0.046)

Table 4: Results from the credible ball simulation study. \mathbf{s}_0 is covered by the horizontal bounds of $B_D(\mathbf{c}_{\text{FOLD}})$ in 89% of replications, despite the point estimator consistently scoring low adjusted Rand index with \mathbf{s}_0 .

(Cacciatore and Tenori, 2022). Figure 12 shows a scatterplot of one example of the `spirals` data. The data is partitioned into $K_0 = 3$ groups, each represented as interlocked spirals. Clustering this data is very difficult because the true clusters have long, thin, non-elliptical shapes, and are quite close to each other in the sample space. Our main interest here is whether $B_D(\mathbf{c}_{\text{FOLD}})$ includes the true grouping of the data, analogous to coverage of a true real parameter by a credible interval.

For each replication, we sample $n = 300$ observations using the `spirals()` function, where each spiral comprises 100 observations. We fit a Bayesian location-scale Gaussian mixture, with $L = 30$, $\mu = 0_d$, $\kappa = 0.5/2$, $\nu = d + 2$, and $\Psi = 0.5\mathbf{I}_d$. The Dirichlet concentration parameter for \mathbf{a} is $\alpha = 1/2$ and we use $\omega = \omega^{\text{AVG}}$ to compute \mathbf{c}_{FOLD} and generate samples from $\Pi(\mathbf{c}_G | \mathbf{X})$. In total, we simulate $R = 100$ replications. In each replication, we run a Gibbs sampler for 15,000 MCMC iterations, discard 1,000 burn-in iterations, and keep every fourth MCMC draw. We compute the credible ball by setting $D(\cdot, \cdot)$ to be the VI.

For these simulations, our main area of interest is whether $\mathbf{s}_0 \in B_D(\mathbf{c}_{\text{FOLD}})$. To do this, we simply evaluate if the horizontal bounds cover \mathbf{s}_0 , that is, if $\text{VI}(\mathbf{s}_0, \mathbf{c}_{\text{FOLD}}) \leq \text{VI}(\mathbf{c}_H, \mathbf{c}_{\text{FOLD}})$, where \mathbf{c}_H is any clustering in $\text{H}(\mathbf{c}_{\text{FOLD}})$. We also saved the number of clusters in \mathbf{c}_{FOLD} and the adjusted Rand index between \mathbf{c}_{FOLD} and \mathbf{s}_0 .

The results are given in Table 4. In 89 of the replications, \mathbf{s}_0 is contained in $B_D(\mathbf{c}_{\text{FOLD}})$, despite \mathbf{c}_{FOLD} consistently underscoring in the adjusted Rand index. This latter phenomena comes about because $E_{\Pi}(\Sigma_l) = 0.5\mathbf{I}_d$, which means that the model is likely to fit Gaussian kernels that span multiple spirals, rather than approximating each spiral with multiple Gaussian kernels. Interestingly, the average number of clusters achieved by \mathbf{c}_{FOLD} is 3.120, which is very close to the truth. We can then conclude that, even when the fitted model makes accurately clustering the data difficult, $\Pi(\mathbf{c}_G | \mathbf{X})$ can still achieve high coverage rates of the truth.

References

- Andrews, T. S. and Hemberg, M. (2019). M3Drop: dropout-based feature selection for scRNAseq. *Bioinformatics*, 35(16):2865–2867.
- Aragam, B., Dan, C., Xing, E. P., and Ravikumar, P. (2020). Identifiability of nonparametric mixture models and Bayes optimal clustering. *The Annals of Statistics*, 48(4):2277–2302.
- Azzalini, A. (2022). *The R Package sn: The skew-normal and related distributions such as the skew-t and the SUN (version 2.1.0)*. Università degli Studi di Padova, Italia.

- Azzalini, A. and Capitanio, A. (1999). Statistical applications of the multivariate skew normal distribution. *Journal of the Royal Statistical Society: Series B (Statistical Methodology)*, 61(3):579–602.
- Azzalini, A. and Valle, A. D. (1996). The multivariate skew-normal distribution. *Biometrika*, 83(4):715–726.
- Barndorff-Nielsen, O. (1965). Identifiability of mixtures of exponential families. *Journal of Mathematical Analysis and Applications*, 12(1):115–121.
- Bartolucci, F. (2005). Clustering univariate observations via mixtures of unimodal normal mixtures. *Journal of Classification*, 22(2):203–219.
- Baudry, J.-P., Raftery, A. E., Celeux, G., Lo, K., and Gottardo, R. (2010). Combining mixture components for clustering. *Journal of Computational and Graphical Statistics*, 19(2):332–353.
- Bensmail, H., Celeux, G., Raftery, A. E., and Robert, C. P. (1997). Inference in model-based cluster analysis. *Statistics and Computing*, 7(1):1–10.
- Binder, D. A. (1978). Bayesian cluster analysis. *Biometrika*, 65(1):31–38.
- Cacciatore, S. and Tenori, L. (2022). *KODAMA: Knowledge discovery by accuracy maximization*. R package version 1.9.
- Cai, D., Campbell, T., and Broderick, T. (2021). Finite mixture models do not reliably learn the number of components. In Meila, M. and Zhang, T., editors, *Proceedings of the 38th International Conference on Machine Learning*, volume 139 of *Proceedings of Machine Learning Research*, pages 1158–1169. PMLR.
- Chan, C., Feng, F., Ottinger, J., Foster, D., West, M., and Kepler, T. B. (2008). Statistical mixture modeling for cell subtype identification in flow cytometry. *Cytometry Part A: The Journal of the International Society for Analytical Cytology*, 73(8):693–701.
- Chen, J. (1995). Optimal rate of convergence for finite mixture models. *The Annals of Statistics*, 23(1):221–233.
- Dahl, D. B., Johnson, D. J., and Müller, P. (2020). *Salso: Search algorithms and loss functions for Bayesian clustering*. R package version 0.2.5.
- Dahl, D. B., Johnson, D. J., and Müller, P. (2022). Search algorithms and loss functions for Bayesian clustering. *Journal of Computational and Graphical Statistics*, 31(4):1189–1201.
- Dang, U. J., Gallagher, M. P., Browne, R. P., and McNicholas, P. D. (2023). Model-based clustering and classification using mixtures of multivariate skewed power exponential distributions. *Journal of Classification*, pages 1–23.
- Di Zio, M., Guarnera, U., and Rocci, R. (2007). A mixture of mixture models for a classification problem: The unity measure error. *Computational Statistics & Data Analysis*, 51(5):2573–2585.

- Duan, L. L. and Dunson, D. B. (2021). Bayesian distance clustering. *Journal of Machine Learning Research*, 22(224):1–27.
- Fraley, C. and Raftery, A. E. (2002). Model-based clustering, discriminant analysis, and density estimation. *Journal of the American Statistical Association*, 97(458):611–631.
- Fritsch, A. (2022). *Mcclust: Process an MCMC sample of clusterings*. R package version 1.0.1.
- Fritsch, A. and Ickstadt, K. (2009). Improved criteria for clustering based on the posterior similarity matrix. *Bayesian Analysis*, 4(2):367–391.
- Genz, A. and Bretz, F. (2009). *Computation of Multivariate Normal and t Probabilities*. Lecture Notes in Statistics. Springer-Verlag, Heidelberg.
- Genz, A., Bretz, F., Miwa, T., Mi, X., Leisch, F., Scheipl, F., and Hothorn, T. (2021). *Mvtnorm: Multivariate normal and t distributions*. R package version 1.1-3.
- Ghosal, S. and Van der Vaart, A. (2017). *Fundamentals of Nonparametric Bayesian Inference*, volume 44. Cambridge University Press.
- Gorsky, S., Chan, C., and Ma, L. (2023). Coarsened mixtures of hierarchical skew normal kernels for flow cytometry analyses. *Bayesian Analysis*, pages 1– 5.
- Guha, A., Ho, N., and Nguyen, X. (2021). On posterior contraction of parameters and interpretability in Bayesian mixture modeling. *Bernoulli*, 27(4):2159–2188.
- Hastie, T., Tibshirani, R., and Friedman, J. H. (2009). *The Elements of Statistical Learning: Data Mining, Inference, and Prediction*, volume 2. Springer.
- Heinrich, P. and Kahn, J. (2018). Strong identifiability and optimal minimax rates for finite mixture estimation. *The Annals of Statistics*, 46(6A):2844–2870.
- Hellinger, E. (1909). Neue begründung der theorie quadratischer formen von unendlichvielen veränderlichen. *Journal für die Reine und Angewandte Mathematik*, 1909(136):210–271.
- Hennig, C. (2010). Methods for merging Gaussian mixture components. *Advances in Data Analysis and Classification*, 4(1):3–34.
- Ho, N. and Nguyen, X. (2016a). Convergence rates of parameter estimation for some weakly identifiable finite mixtures. *The Annals of Statistics*, 44(6):2726–2755.
- Ho, N. and Nguyen, X. (2016b). On strong identifiability and convergence rates of parameter estimation in finite mixtures. *Electronic Journal of Statistics*, 10(1):271–307.
- Ho, N., Nguyen, X., and Ritov, Y. (2020). Robust estimation of mixing measures in finite mixture models. *Bernoulli*, 26(2):828–857.
- Ishwaran, H. and James, L. F. (2001). Gibbs sampling methods for stick-breaking priors. *Journal of the American Statistical Association*, 96(453):161–173.

- Ishwaran, H. and James, L. F. (2003). Some further developments for stick-breaking priors: Finite and infinite clustering and classification. *Sankhyā: The Indian Journal of Statistics (2003-2007)*, 65(3):577–592.
- Jain, A. K. (2010). Data clustering: 50 years beyond K-means. *Pattern Recognition Letters*, 31(8):651–666.
- Jain, S. and Neal, R. M. (2004). A split-merge Markov chain Monte Carlo procedure for the Dirichlet process mixture model. *Journal of Computational and Graphical Statistics*, 13(1):158–182.
- Jain, S. and Neal, R. M. (2007). Splitting and merging components of a nonconjugate Dirichlet process mixture model. *Bayesian Analysis*, 2(3):445–472.
- Juárez, M. A. and Steel, M. F. (2010). Model-based clustering of non-Gaussian panel data based on skew-t distributions. *Journal of Business & Economic Statistics*, 28(1):52–66.
- Karlis, D. and Santourian, A. (2009). Model-based clustering with non-elliptically contoured distributions. *Statistics and Computing*, 19(1):73–83.
- Kiselev, V. Y., Andrews, T. S., and Hemberg, M. (2019). Challenges in unsupervised clustering of single-cell RNA-seq data. *Nature Reviews Genetics*, 20(5):273–282.
- Krijthe, J. H. (2016). RSSL: R package for semi-supervised learning. In *Reproducible Research in Pattern Recognition. RRPR 2016. Lecture Notes in Computer Science, vol 10214*, pages 104–115.
- Krijthe, J. H. and Loog, M. (2015). Implicitly constrained semi-supervised least squares classification. In *14th International Symposium on Advances in Intelligent Data Analysis XIV (Lecture Notes in Computer Science Volume 9385)*, pages 158–169.
- Lau, J. W. and Green, P. J. (2007). Bayesian model-based clustering procedures. *Journal of Computational and Graphical Statistics*, 16(3):526–558.
- Li, H., Courtois, E. T., Sengupta, D., Tan, Y., Chen, K. H., Goh, J. J. L., Kong, S. L., Chua, C., Hon, L. K., Tan, W. S., et al. (2017). Reference component analysis of single-cell transcriptomes elucidates cellular heterogeneity in human colorectal tumors. *Nature Genetics*, 49(5):708–718. PMID: 28319088.
- Li, J. (2005). Clustering based on a multilayer mixture model. *Journal of Computational and Graphical Statistics*, 14(3):547–568.
- Lun, A. T., Bach, K., and Marioni, J. C. (2016). Pooling across cells to normalize single-cell RNA sequencing data with many zero counts. *Genome Biology*, 17(1):1–14.
- Malsiner-Walli, G., Frühwirth-Schnatter, S., and Grün, B. (2017). Identifying mixtures of mixtures using Bayesian estimation. *Journal of Computational and Graphical Statistics*, 26(2):285–295.

- Manole, T. and Ho, N. (2022). Refined convergence rates for maximum likelihood estimation under finite mixture models. In Chaudhuri, K., Jegelka, S., Song, L., Szepesvari, C., Niu, G., and Sabato, S., editors, *Proceedings of the 39th International Conference on Machine Learning*, volume 162 of *Proceedings of Machine Learning Research*, pages 14979–15006. PMLR.
- Manole, T. and Khalili, A. (2021). Estimating the number of components in finite mixture models via the group-sort-fuse procedure. *The Annals of Statistics*, 49(6):3043–3069.
- McInnes, L., Healy, J., Saul, N., and Großberger, L. (2018). UMAP: Uniform manifold approximation and projection. *Journal of Open Source Software*, 3(29):861.
- Medvedovic, M. and Sivaganesan, S. (2002). Bayesian infinite mixture model based clustering of gene expression profiles. *Bioinformatics*, 18(9):1194–1206.
- Meilă, M. (2007). Comparing clusterings—an information based distance. *Journal of Multivariate Analysis*, 98(5):873–895.
- Melnykov, V. (2016). Merging mixture components for clustering through pairwise overlap. *Journal of Computational and Graphical Statistics*, 25(1):66–90.
- Miller, J. W. and Dunson, D. B. (2019). Robust Bayesian inference via coarsening. *Journal of the American Statistical Association*, 114(527):1113–1125.
- Miller, J. W. and Harrison, M. T. (2013). A simple example of Dirichlet process mixture inconsistency for the number of components. In Burges, C., Bottou, L., Welling, M., Ghahramani, Z., and Weinberger, K., editors, *Advances in Neural Information Processing Systems*, volume 26. Curran Associates, Inc.
- Miller, J. W. and Harrison, M. T. (2014). Inconsistency of Pitman-Yor process mixtures for the number of components. *The Journal of Machine Learning Research*, 15(1):3333–3370.
- Miller, J. W. and Harrison, M. T. (2018). Mixture models with a prior on the number of components. *Journal of the American Statistical Association*, 113(521):340–356.
- Neal, R. M. (2000). Markov chain sampling methods for Dirichlet process mixture models. *Journal of Computational and Graphical Statistics*, 9(2):249–265.
- Nguyen, X. (2013). Convergence of latent mixing measures in finite and infinite mixture models. *The Annals of Statistics*, 41(1):370–400.
- O’Hagan, A., Murphy, T. B., Gormley, I. C., McNicholas, P. D., and Karlis, D. (2016). Clustering with the multivariate normal inverse Gaussian distribution. *Computational Statistics & Data Analysis*, 93:18–30.
- Paganin, S., Herring, A. H., Olshan, A. F., and Dunson, D. B. (2021). Centered partition processes: Informative priors for clustering (with discussion). *Bayesian Analysis*, 16(1):301 – 670.

- Pitman, J. (1995). Exchangeable and partially exchangeable random partitions. *Probability Theory and Related Fields*, 102(2):145–158.
- Rand, W. M. (1971). Objective criteria for the evaluation of clustering methods. *Journal of the American Statistical Association*, 66(336):846–850.
- Redner, R. A. and Walker, H. F. (1984). Mixture densities, maximum likelihood and the EM algorithm. *SIAM Review*, 26(2):195–239.
- Rigon, T., Herring, A. H., and Dunson, D. B. (2023). A generalized Bayes framework for probabilistic clustering. *Biometrika*.
- Rodríguez, C. E. and Walker, S. G. (2014). Univariate Bayesian nonparametric mixture modeling with unimodal kernels. *Statistics and Computing*, 24(1):35–49.
- Rousseau, J. and Mengersen, K. (2011). Asymptotic behaviour of the posterior distribution in overfitted mixture models. *Journal of the Royal Statistical Society: Series B (Statistical Methodology)*, 73(5):689–710.
- Scrucca, L., Fop, M., Murphy, T. B., and Raftery, A. E. (2016). Mclust 5: Clustering, classification and density estimation using Gaussian finite mixture models. *The R Journal*, 8(1):289–317.
- Teicher, H. (1961). Identifiability of mixtures. *The Annals of Mathematical Statistics*, 32(1):244–248.
- Tortora, C., Franczak, B. C., Browne, R. P., and McNicholas, P. D. (2019). A mixture of coalesced generalized hyperbolic distributions. *Journal of Classification*, 36(1):26–57.
- Wade, S. (2015). *Mclust.ext: Point estimation and credible balls for Bayesian cluster analysis*. R package version 1.0.
- Wade, S. and Ghahramani, Z. (2018). Bayesian cluster analysis: Point estimation and credible balls (with discussion). *Bayesian Analysis*, 13(2):559–626.